Mon. Not. R. Astron. Soc. **000**, 1–16 (2009) Printed 20 July 2010 (MN LATEX style file v2.2)

Spectroscopy and kinematics of low-mass members of young moving groups

M. C. Gálvez-Ortiz,[1⋆] J. R. A. Clarke,[1] D. J. Pinfield,[1] J. S. Jenkins,[2], S. L. Folkes,[1] A. E. García Pérez,[3] A. C. Day-Jones,[2] B. Burningham,[1] H. R. A. Jones,[1] J.R. Barnes,[1] and R.S. Pokorny[4]

[1] *Centre for Astrophysics Research, Science and Technology Research Institute, University of Hertfordshire, Hatfield AL10 9AB, UK*
[2] *Department of Astronomy, Universidad de Chile, Casilla Postal 36D, Santiago, Chile*
[3] *Department of Astronomy, University of Virginia, P.O. Box 400325, Charlottesville, VA 22904-4325, USA*
[4] *Yunnan Observatory, P.O. Box 110. CAS. 650011 Kunming. P. R. China.*

Accepted. Received ;

ABSTRACT

We study a target sample of 68 low-mass objects (with spectral types in the range M4.5-L1) previously selected via photometric and astrometric criteria, as possible members of five young moving groups: the Local Association (Pleiades moving group, age=20 - 150 Myr), the Ursa Mayor group (Sirius supercluster, age=300 Myr), the Hyades supercluster (age=600 Myr), IC 2391 supercluster (age=35 - 55 Myr) and the Castor moving group (age=200 Myr). In this paper we assess their membership by using different kinematic and spectroscopic criteria. We use high resolution echelle spectroscopic observations of the sample to measure accurate radial velocities (RVs). Distances are calculated and compared to those of the moving group from the literature, we also calculate the kinematic Galactic components (U,V,W) of the candidate members and apply kinematic criterion of membership to each group. In addition we measure rotational velocities ($v \sin i$) to place further constraints on membership of kinematic members. We find that 49 targets have young disk kinematics and that 36 of them possibly belong to one of our five moving groups. From the young disk target objects, 31 have rotational velocities in agreement with them belonging to the young disk population. We also find that one of our moving group candidates, 2MASS0123-3610, is a low-mass double lined spectroscopic binary, with probable spectral types around M7.

Key words: stars: low-mass, brown dwarfs – stars: kinematics

1 INTRODUCTION

Ultracool dwarfs (UCDs) include objects with spectral type of M7 or later (corresponding to Teff<2500K). Many of these objects have been identified in recent and ongoing large area surveys (i.e. 2MASS, SDSS, UKIDSS). However, the physics of their cool atmospheres, as well as their kinematic properties are not yet fully known. UCDs have complex atmospheres, the spectra of which are dominated by molecular bands and dust. Theory and observation clearly suggest that the spectra of these objects are significantly effected by gravity and metallicity (e.g. Knapp et al. 2004, Burgasser al. 2006), but current model spectra cannot fit these parameters (Lyubchik et al. 2007). UCDs whose properties can be inferred without atmospheric models would give us rigorous test-bed for theory and vital information about how the physical properties affect the spectra.

One variety of benchmark UCD is in binary systems, since UCD properties may be constrained by the primary star (e.g. Day-Jones et al. 2008; Zhang et al. 2010; Burningham et al. 2010). Other way to obtain such *benchmark* objects is to find members of known, characterised moving groups.

A classical moving group (MG), as defined by Eggen (1984a,b), is a young stellar population that shares a common space motion (e.g. Pinfield et al. 2006). MGs form when the gas remnants of a star-forming cloud are cleared (by hot star action) and many of the stars become unbound. This population slowly disbands (at a few kms^{-1}), but maintains its bulk space motion for up to ∼1 Gyr before being dispersed by disk heating mechanisms (De Simone et al. 2004). MGs may leave behind a bounded core of stars that

⋆ E-mail:M.Galvez-Ortiz@herts.ac.uk

become open clusters, so young open clusters are often in MGs. Because of their common origin, MG members have a shared age and composition, which can be well constrained by studies of high mass members or associated open clusters (Barrado Y Navacués et al. 1999). MGs thus represent young coeval populations with well constrained ages, and because they are dispersed through space, they can be relatively nearby. These nearby UCD young MG members are also optimal targets for faint companion searches, in particular, for high resolution imaging searches where the more manageable brightness ratio between primary and secondary would favour identification (e.g. Jenkins et al. 2010).

However, recent studies, (Famaey et al. 2007, 2008; Antoja et al. 2008; Klement et al. 2008; Francis & Anderson 2009; Zhao et al. 2009; López-Santiago et al. 2009), seem to support a dynamic or resonant mechanism origin of MGs or find a high percentage of contamination of old field stars. Mayor (1972) and Kalnajs (1991) suggested a different dynamic origin of MGs. Dehnen (1998) pointed out that the origin of most MGs could be caused by orbital resonances and Skuljan et al. (1999) related the origin to the Galactic spiral structure, or to some other global characteristic of the Galactic potential, combined with the initial velocities of the stars. But both hypothesis, that kinematic groups are cluster remnants or that MGs origin are dynamic, are compatible.

Some authors have studied the contamination of young MGs by older field stars. López-Santiago et al. (2009) analysis of a late type kinematic member sample indicates that the contribution of old field stars to the sample of candidates of Local Association MG was ≈50%, with similar results in the Pleiades MG by Famaey et al. (2008). Due to this, spectroscopic complementary studies of youth signatures is crucial to assess the kinematic membership. The combined information of kinematic and spectroscopic signatures of youth will provide a confident member sample.

The best documented groups are the Hyades supercluster (Eggen 1992b) associated with the Hyades cluster (600 Myr), the Ursa Mayor group (Sirius supercluster) (e.g. Eggen 1984a, 1998b, Soderblom & Mayor 1993a, b) associated with the UMa cluster (300 Myr), IC 2391 supercluster (35-55 Myr) (Eggen 1991, 1995), the Castor Moving Group (200 Myr) (e.g. Barrado y Navascués 1998), and the Local Association (20-150 Myr) or Pleiades moving group (a coherent kinematic stream of young stars with embedded clusters and associations such as the Pleiades, α Per, IC 2602, etc) (Eggen 1983, 1992c).

In this paper we present the second stage of a major survey of UCDs in moving groups (building in the work presented in Clarke et al. 2010, hereafter Paper I). We centre here on the results obtained in a study of the candidate MG members using high resolution spectra to access their kinematic signatures and resulting MG membership criteria.

In Section 2 we describe the sample selection. In Section 3 we give the details of our observations and our data reduction techniques. In Section 4 we present the new parameters obtained for our sample. In Section 5 we assess our candidates properties in the context of MG membership. Finally, in Section 6 we give a brief summary and the near future prospects for improved measurements.

2 SAMPLE SELECTION

The sample presented here was selected from Paper I where we used photometric and astrometric criteria in order to search for UCD in moving groups. We combined an extended version of the Liverpool-Edinburgh High Proper Motion survey (ELEHPM) and Southern Infrared Proper Motion Survey (SIPS) with the Two Micron All Sky Survey (2MASS), and applied colour cuts of J-K_s $\geqslant$1.0 and R-K_s $\geqslant$5.0 to select objects with spectral type predominantly later than M6. We selected objects from both catalogues where $\mu/\Delta\sigma_\mu > 4$ (μ is proper motion and σ_μ is the proper motion one sigma uncertainty) to ensure proper motion accuracy.

Our final red object catalogue was made up of 817 objects. By using both astrometric and photometric criteria, we concluded that 132 of these objects were possible members of one or more of the five MGs in study. The application of these criteria is detailed in Paper I. We perform high resolution follow up of a representative subset of this sample, all with spectral types in the range M4.5-L1 and with ≈45% of the sample being M7 or later.

3 OBSERVATIONS AND REDUCTION

In this paper we analysed optical and near infrared high resolution echelle spectra of 68 objects. The data were obtained during four observing runs detailed in Table 1.

The UVES (Dekker et al. 2000) spectra were extracted using the standard reduction procedures in the IRAF[1] echelle package (bias subtraction, flat-field division, extraction of the spectra, telluric correction and calibration). We obtained the wavelength calibration by taking spectra of a Th-Ar lamp. The average signal-to-noise of the data, measured as the square root of the signal, in these runs is ≈22.

Whilst the wavelength coverage of these runs is ample, low signal-to-noise due to poor efficiency at the echellogram ends renders portions of the spectrum unusable. As a result, it was not possible to measure certain important features such as the Li I λ6707 Å absorption line.

A similar procedure was followed for the Phoenix data. The observations in this case were made in a set of subexposures in an ABBA jitter pattern to facilitate background subtraction. Due to the lack of Th-Ar lamp, the wavelength calibration was done using sky lines in every spectrum with sufficient signal in the sky. For the objects with low signal in the sky, we used the spectra of a giant star (HR 5241). The average signal-to-noise of the data in this run is ≈15.

In the case of FEROS (Kaufer et al. 1999) data, Starlink software was used for bias subtraction, flat-field division and optimal spectra extraction. The extracted spectra were wavelength calibrated using the Th-Ar illuminated images obtained after each observation. The average signal-to-noise of the data in this run is ≈25. For details of our FEROS reduction see Paper I.

[1] IRAF is distributed by the National Optical Observatory, which is operated by the Association of Universities for Research in Astronomy, Inc., under contract with the National Science Foundation.

4 MEASUREMENTS OF PARAMETERS

4.1 Spectral Types and distances

We performed a simple analysis to obtain the objects' spectral types. We measured the PC3 index as defined in Martín et al. (1999) and applied the index-spectral type relation to derive a spectral type. We measured also TiO5 and VO-a indexes as defined in Cruz & Reid (2002). We derived spectral type from TiO5 following the double valued relation given in Cruz & Reid (2002), using the relation for Ti05<0.75, except for object with spectral type later than M7 were we used the relation given for Ti05>0.30. We also derived a spectral type from VO-a index following the relation gives in Cruz & Reid (2002) for the correspondent spectral type interval. We took as definitive spectral type the average of these three spectral types rounded to the closest 0.5 class. When one of the spectral areas covered by these indexes were no usable we make the average between the other two. The spectral type estimated error is ≈1.0 spectral class derived from these relations.

Due to the wavelength range of the Phoenix data, we can not measure PC3, so we measure the spectral types instead using the I-J colour index-spectral type relation from Leggett (1992).

We then calculated a more accurate spectroscopic distance using a PC3-absolute J-magnitude relation from Crifo et al. (2005). The error in distance following Crifo is 12%. For Phoenix data, distances were calculated from the absolute J magnitude-spectral type relation from Dahn et al. (2002). The spectral classification and distances are given in Table 2, where previous known data from the literature is also given. The values in both sets are in agreement except for two objects, 2MASS J0334-2130 and SIPS 1632-0631, that differ in more than one spectral type and SIPS2039-1126 that differ one spectral type. The value from the literature for 2MASS J0334-2130 and SIPS 2039-1126 classification comes from Cruz et al. (2003), where all spectral types for M dwarfs were determined via visual comparison with standard star spectra taken during the course of the program (the objects were typed by being normalised and plotted between spectra from a grid of eight standard M1-M9 dwarfs from Kirkpatrick, Henry & McCarthy 1991). In this case we think our index average measurements will give more accurate spectral types. For SISPS 1632-0631, we took the spectral type from Gizis (2002), where the final classification comes from the measurements of several spectral indexes (including TiO5, PC3, CrH, TiO-b and visual inspection). The PC3 and TiO5 in Gizis (2002) (1.99, 0.25) are very similar to the ones calculated by us (1.95, 0.26), but our value of VO-a (2.35) is the double of Gizis's (1.14). Although Gizis (2002) takes an average of six indicators while we only take three, we rely on our classification. As we mentioned above, the spectral type-index relation of TiO5 and VO-a indexes in the Cruz & Reid (2002) is double value with a turning around M7 and M9 for TiO5 and VO-a respectively, that is that there is a different relation for objects with spectral type under or over around M7 for TiO5 and M9 for VO-a. SIPS 1632-0631 is just in the M7-M9 limit. We find that the best agreement in the spectra type with PC3 is when we used the relation for >M7 in TiO5 and for <M9 in VO-a, giving same spectral type, M8.5, for the three indexes.

Due to the spectroscopic binarity, as we will see in Sect. 5.3 or possible binarity without confirmation of some object in the sample we expect that the error in the indexes spectral types and distances are larger than the ones shown in Table 2.

To obtain spectral types for our FEROS objects we initially used the PC3 index from Martín et al. (1999), however this coincided often with a unusable region of spectra. We thus used the VO index from Kirkpatrick, Henry & Simons et al (1995), CaH from Kirkpatrick, Henry & McCarthy (1991), VO-a and TiO5 from Cruz & Reid (2002) and PC3, TiO1+TiO2 and VO1+VO2 from Martín et al. (1999) to create a mean spectral type (see Paper I for details).

4.2 Radial velocities

The heliocentric radial velocities have been determined by using the cross-correlation technique. The spectra of the targets were cross-correlated order by order, by using the routine FXCOR in IRAF, against spectra of radial velocity standards with similar spectral type.

The radial velocity was derived for each order from the position of peak of the cross-correlation function peak (CCF), and the uncertainties were calculated by FXCOR based on the fitted peak height and the antisymmetric noise as described by Tonry & Davis (1979).

In the case of the FEROS data, we cross-correlated each individual order of the reduced spectra using an IDL routine that determines the cross-correlation of two arrays and finds the maximum cross-correlation function by fitting a Gaussian to the central peak. Our final radial velocities and associated uncertainties came from the mean and standard deviation of these measurements. A heliocentric correction was made to the measured shift between the object and the reference star so that the we could calculate radial velocities with respect to the Sun.

In Table 3 we give the information about the reference stars used in every run. The object LP 944-20 exhibits ∼3.5 km s^{-1} radial velocity variability, as is shown in Martín et al. (2006), so when we had another radial velocity template in the run we checked the velocity of LP 944-20 with respect to this other template and found good agreement within the uncertainties.

In Table 4 we list, for each spectrum, the heliocentric radial velocities (V_r) and their associated uncertainties (σ_{V_r}) obtained as weighted means of the individual values deduced for each order used. Those orders which contain chromospheric features and prominent telluric lines have been excluded. In the case of Phoenix data, the signal-to-noise of the spectra is low and so we decided to add an uncertainty deduced from the variation found in the standard stars calibrations (LP 944-20 and GL 406 in this case).

For the binary case (2MASS0123-3610), we have to take into account an additional uncertainty due to the systematic distortion of the peak from the presence of a companion.

4.3 Space motions

To constrain space motions, we obtained a number of distances depending of potential MG membership for each object with radial velocity measure.

As detailed in Paper I, to allow for younger objects appearing intrinsically brighter, we created isochrones corresponding to the ages of our MGs and that of a field dwarf using atmospheric models from Baraffe et al. (1998). According to each object's candidature group membership from photometric and astrometric criteria, the difference in absolute J-magnitude of each object is used in Dahn et al. (2002) distance-spectral type relation to give a new corrected distance assuming group membership. This way we obtained a number of distances for each of the objects.

Using these distances or any parallaxes available from the literature, the proper motion data, and the radial velocities calculated in Sect. 4.2, we computed the Galactic space-velocity components (U, V, W) of the sample by using the transformation matrices of Johnson & Soderblom (1987). Positive U is towards the Galactic centre, positive V is in the direction of Galactic rotation, and positive W is in the direction of the Galactic north pole.

The resulting values of (U, V, W) according to potential group membership and associated errors are given in Table 4. In the table, the objects that appear to be kinematic members, that is, that are in agreement with the membership, are highlighted in bold (see Section 5).

4.4 Rotational velocities

To determine rotational velocities we made use of the cross-correlation technique in our high resolution echelle spectra by using the routine FXCOR in IRAF.

When a stellar spectrum with rotationally broadened lines is cross-correlated against a narrow-lined spectrum, the width of the cross-correlation function (CCF) is sensitive to the amount of rotational broadening of the first spectrum. Thus, by measuring this width using Gaussian profiles, one can obtain a measurement of the rotational velocity of the star. The target spectra were cross-correlated against the spectrum of the template stars. We give the data of the templates used in each run in Table 3. The templates should be of equal or similar spectral types as the targets, but an M-type template can be used for all M type dwarfs (see e.g. Bailer-Jones 2004; Zapatero-Osorio 2006), therefore as our targets and references are all in M4-M9 range, we applied our templates to all stars.

The calibration of the width (FWHM) of the templates to yield an estimation of $v \sin i$ is determined by cross-correlating artificially broadened spectra of the template star with the original template star spectrum. We rotate them up to 100 km s^{-1} in 1 km s^{-1} steps. The broadened spectra were created for $v \sin i$ is spanning the expected range of values by convolution with a theoretical rotational profile (Gray 1992) using the program STARMOD (developed at Penn State University; Barden 1985) and the *vsini* routine of the SPECTRUM synthesis code (Richard O. Gray, 1992-2008). The resultant relationship between $v \sin i$ and FWHM of the CCF was fitted with a fourth-order polynomial. This method should not be used at rotational velocities greater than around 50 km s^{-1} since the CCF profiles radically differ from Gaussianity. Therefore, in our rotational range of interest, $5 > v \sin i > 50$, the fit is good. We used several spectral ranges for these measurements. As mentioned in Reiners & Basri (2008), absorption band of FeH around 1μm is a rich area in ultracool stars, free of telluric absorption and is not pressure-broadened, but the spectra that we had covering that area (UVES data) present an artifact that do not allow us to make any measurements with the reliability needed. So, we use that band only to check the values obtained in other areas.

The rotational velocities given in the 8th column of Table 4 are the average of the values measured when more than one template star was used.

The uncertainties on the $v \sin i$ values obtained by this method have been calculated using the parameter R defined by Tonry & Davis (1979) as the ratio of the CCF height to the rms antisymmetric component. This parameter is computed by the task FXCOR and provides a measure of the signal-to-noise ratio of the CCF. Tonry & Davis (1979) showed that uncertainties in the FWHM of the CCF are proportional to 1/(1 + R) and Hartmann et al. (1986) and Rhode et al. (2001) found that the quantity $v \sin i[1/(1 + R)]$ provides a good estimate for the 90% confidence level of any $v \sin i$ measurement using this methodology. This error, $v \sin i[1/(1 + R)]$, should be a reasonable estimate of the uncertainties on our $v \sin i$ measurements. Nevertheless, we estimate the uncertainties to be at least 3 km s^{-1} for all values, which is the level of variation presented by the reference stars. The reason is that the main source of uncertainty comes from the low signal-to-noise of the spectra and so is not reflected properly in the statistical results of the calculations.

Taking into account the resolution of our spectra, the rotation of our templates (see Table 3) and the signal-to-noise, we consider that the minimum detectability value of $v \sin i$ would be in the range ≈6-10 km s^{-1}. Thus, we have assumed a general limit of 10 km s^{-1}. All data below this limit would be marked as $v \sin i \leqslant 10$ km s^{-1} in Table 4.

5 ANALYSIS

5.1 Space motions and kinematics

We apply a simple kinematic criterion to distinguish old and young disk objects in our sample of 68 objects with high resolution spectra.

In Figure 1, we plot the UV and WV planes for the whole sample including the boundaries (continuous line) that determine the young disk population as defined by Eggen (1984a,b, 1989). We then classify objects as young disk (YD) if they lie within the young disk region in the UV plane (or if they could, given U and V 1σ errors). Objects whose location in the UV plane is inconsistent with YD membership are all consistent with an old disk (OD) classification.

If we follow Legget (1992) criterion, the sample should be divided into young disk (YD), old disk (OD), young-old disk (YO), old-disk halo (OH) and halo (H) objects: all stars with V < -100, or with an eccentricity in the UV plane >>0.5, were defined as H; objects with an eccentricity in the UV plane of ≈0.5 were defined as OH; stars within the young disk region in the UV plane, approximately defined by -20 < U < 50, -30 < V < 0, and with -25 < W < 10, were defined as YD; objects with an eccentricity in the UV plane less than 0.5, that lie outside the young disk region, or that lie within the young disk region but have $|W| > 50$, were

defined as OD. Finally, objects that lie around the edge of the young disk region or lie within the area with $|W| < 50$ but greater than that required for classification as YD, were defined as YO. However, in our sample all the objects would be classified by young disk or old-young disk membership, (see Fig. 1 and W value in Table 4), and will refer to them as YD and OD for simplicity.

In addition we identify possible members of the five MGs by their relative position in the UV and VW diagrams (Fig. 1) with respect to the boxes (dashed lines) that mark the velocity ranges of each MG. The centre of the five main MGs are marked (with large open symbols) and our kinematic members are shown as corresponding filled symbols. The boxes are defined by studies with samples of higher mass members from the literature (Barrado Y Navacués 1998; Montes et al. 2001). See Paper I for a detailed description. As mentioned above, a kinematic member was defined as either lying inside the relevant box in each diagram, or having uncertainties that overlapped appropriately. Objects inside YD boundaries should be young although it is not clear that they belong to an established MG.

According to their kinematic behaviour, we have 49 objects that belong to the young disk area, and 36 of them are candidates members of one of the five MGs. Some objects are candidates for more than one MG (see Table 5). We find seven possible candidates to Castor, 25 to Hyades, seven to IC 2391, five to Pleiades and none to Sirius. Eleven objects belong to young disk region without clear membership to any of these five MGs.

These new candidates represent a significant addition to the low-mass membership of several MGs that for the most part have few low-mass members confirmed to date, and provide a corresponding improvement in any determination of the low-mass initial mass function (IMF). Our seven candidate members of the Castor MG represent an increase of 10% in the total known membership (see e.g. Caballero 2010), and an increase of 50% in the very low-mass regime. The Hyades group presents a deficiency of very low-mass objects (15 of ≈500 stars). Bouvier et al (2008) suggest that the Hyades originally had 150-200 brown dwarfs (BDs) compared to its current 10-15, based on the assumption that the Hyades is a dynamically evolved version of the Pleiades and considering the two clusters present mass functions over the 0.005-3$M_\odot$ range. Hogan et al (2008) reported 12 new L dwarf Hyades members (estimating ≈20% contamination). Here we present 25 low-mass candidates which, if confirmed, will further aid our understanding of the evaporation of young clusters. IC 2391 as well as other young clusters present also a brown dwarf deficit, that might be explained by an onset of larger-size dust grain formation in the upper atmosphere of objects with spectral types M7-M8 or later (Dobbie et al. 2002; Jameson et al. 2003; Barrado Y Navacués et al. 2004; Spezzi et al. 2009). From 180 members around a dozen are substellar (Spezzi et al. 2009), a low number from which to draw a statistically significant conclusion. Although our candidates are M4.5-M7 spectral type, they increase the low-mass population and favour future statistics. Pleiades is a very well studied and populated cluster and many works have undertook the low-mass and BD population search and IMF study (e.g. Londieu et al. 2007), our five candidates are in M6-M8.5 spectral type and will contribute to populate this spectral type range.

We have to keep in mind that contamination of the young disk space velocity area by old field population occurs. It has been studied in several kinematic moving groups as we mentioned in the introduction, concluding that a high percentage of contamination happens (e.g. López-Santiago et al. 2009 and reference therein). So the next logical step is to further asses the kinematic candidates found with additional information, such as the study of several youth indicators, to confirm their membership.

5.2 Rotational velocity-spectral type relation

The rotational evolution of low-mass object is complicated. Several studies have demonstrated that after becoming a fully convective object (spectral types later than ≈M3), when gravitational contraction is finished, rotational braking is present at least in all M type objects. The spin-down times are longer for Late M dwarfs than for earlier M types (e.g. Zapatero-Osorio et al. 2006; Reiners & Basri 2008, Jenkins et al. 2009). Jenkins et al. (2009) show a statistical relationship between mid/late type M dwarf rotation and age and hence taking all these works together we can use rotational velocity as a way to differentiate between young and older M type UCD populations. As demonstrated in Figs. 9 and 10 of Reiners & Basri (2008), such populations occupy distinct regions of the $v \sin i$-spectral type diagram depending on its age, with the older objects concentrated in an "envelope of minimum rotation velocity". Even for the latest M dwarfs this envelope corresponds to a fairly low rotation rate ($v \sin i < 20$ km s^{-1}). The model overlays that Reiners & Basri (2008) derive (based on a breaking law fit to the overall observed population) that the great majority of mid-late field M dwarfs (e.g. with ages ∼2-10 Gyr) have $v \sin i < 30$ km s^{-1}, and that younger objects of this type should be much more rapid rotators ($v \sin i$ = 30-100 km s^{-1}). Although the random inclination of rotation axis can reduce measured $v \sin i$, it seems clear that rotational velocity constraints can provide a very helpful complement to our kinematic membership.

One Reiner & Basri (2008) result is that the rotational evolution according to a wind-braking law that scales with temperature can reproduce better the observational data for L dwarfs. While for M dwarfs both rotational evolution according to a wind-braking law that scales with temperature or with mass are very similar. We choose the first one here although this is a moot point since both models give similar results over our spectral type range. In Fig. 2 we plot spectral type versus $v \sin i$. On the left, we plot our sample with Reiners & Basri (2008) Figure 10. Circles are from them and open triangles from Zapatero-Osorio et al. (2006). Following Reiners & Basri (2008), filled blue circles are probably young, filled red circles old and open circles have no age information. Our sample data is plotted as different symbols depending if they have been classified as YD or OD. As in Reiners & Basri (2008), we mark in dashed lines ages of 2, 5 and 10 Gyr (from upper left to lower right). To obtain a criterion to separate objects of differing age, we plot in blue a continuous line: the "apparent" separation between a "young" and "old" object and so use it as an indicator of MG membership for our targets. We include LP 944-20 in the plot as it shows a strong candidature to be a member of Castor MG (see Ribas 2003b for details). It is plotted as an

arrow with our measured value of $v \sin i$, in agreement with previous works (see Table 3) and with being young. On the right side we show a zoom version where we plot the targets in different symbols, which indicate for which MG they are candidate members. In this case we do not plot literature data for clarity. Note that the objects marked as <10 km s^{-1} in Table 4 are plotted with this value in Fig. 2, so this should mark an upper limit of rotational rate.

We measure the rotational velocity of 54 of the 68 objects in the sample, and of 42 of the 49 YD objects. From these 42, we find that 31 present a projected rotational velocity in agreement with our criterion of youth and 12 that can not be dismissed as they have velocities in the limit between both populations or we have no rotational velocity information.

Despite being outside the young disk region, 10 objects have youthful rotational velocities. Uncertainties in the (U, V, W) measurements would be compounded by possible binarity among older objects which can allow them to keep high rotation rates longer that in case of singles.

Table 5 sums up these results. The first and second columns are name and kinematic classification. Third column classifies the objects as young (Y) if they lie in the upper part of the limiting line, old (O) if they lie under the line and unknown age (Y-O) if they are in the limit of both areas or the rotational velocity superior limit is not clear enough to classify them in one of the groups. Column four highlights to which MG the candidates are kinematic members. In this case, HY for Hyades, SI for Sirius, CA for Castor, PL for Pleiades and IC for IC 2391, and OYD for other young disk members without a membership of one of the five MG in consideration. The confirmed 31 YD members objects are highlighted in bold in Table 5, and the 12 more including as possible members are highlighted in bold with a question mark. Only two objects that presented candidature to any of the MGs have been dismissed due to the rotational velocity and have a (N) in Table 5.

As we have used the projected rotational velocity for our study, the real rotational velocity can only be higher and so the objects over our youth limit will stay there, but the dispersion introduced by the inclination and the fact that the rotation rate can be influenced by other external factors, like binarity, make us use this method only as a supporting criterion.

Five objects of our list, DENIS0041-5621, 2MASSJ0429-3123, SIPS0440-0530, 2MASSJ1507-2000 and DENIS2200-3038, overlap with Reiners & Basri (2009) and Seifahrt et al. (2010). The kinematic shows they are YD except for 2MASSJ1507-2000, while two of them show MG candidature, SIPS0440-0530 and DENIS2200-3038. DENIS0041-5621 shows evidence of accretion and presence of Li I 6708 Å, which implies that it is very young (Reiners & Basri 2009). We had classified this object as other young disk, as it is kinematically young and the rotational velocity is in agreement. 2MASSJ0429-3123 shows no Li I in Reiners & Basri (2009). We have this object classified as YD due to kinematics but the rotational velocity indicate it could be old, classified as an M7.5 with no lithium, it is probably an old object. SIPS0440-0530 is classified by us as a young object member of Hyades MG. Reiners & Basri (2009) found no Li I but this could be compatible with being a HY member. Hα and other indicators of activity will give us more information as it is M7.0 spectral type. 2MASSJ1507-2000 shows quite different radial velocity measurement in Reiners & Basri (2009) (-2.5 km s^{-1} instead of our -22.18 km s^{-1}), we can not explain this difference, the additional error maybe produced by low signal-to-noise spectra is not enough for producing this discrepancy. This object is kinematically classified as OD and also shows no Li I in Reiners & Basri (2009). DENIS2200-3038 is kinematically classified as Hyades member, which is consistent with the findings of Seifahrt et al. (2010), but with M9 spectral type the rotation criterion gives an old object. Further spectroscopic criteria is needed to confirm these results.

5.3 SB2 type binarity: 2MASS0123-3610

Multiplicity of stars can yield dynamical mass constraints, as well as being an important constraint of stellar formation and evolution. The properties of multiple stellar systems have long provided important empirical constraints for star formation theories. Binary properties of the low-mass stars of FGK and early M spectral types have been extensively studied (e.g., Duquennoy & Mayor 1991 and Fischer & Marcy 1992). But, despite the interest in the multiplicity of very low mass objects (stars at the bottom of the main sequence and brown dwarfs) in recent years (e.g. Martín et al. 2003; Close et al. 2003, 2007; Gizis et al. 2003; Pinfield et al. 2003; Basri & Reiners 2006; Reid et al. 2006; Ahmic et al. 2007; etc), and the subsequent progress in finding and characterising them, very few direct measurements of their physical properties have been made, in particular dynamical masses (e.g. Zapatero Osorio et al. 2004, Dupuy et al. 2009a and Dupuy et al. 2009b), and our understanding of their formation processes is not clear.

Double (or multiple) lined spectroscopic binaries (SBs) allow precise determination of dynamical properties of the components, including the mass ratio and, if the inclination can be determined, the individual component masses.

During the reduction process of our sample we find some objects that show possible spectroscopic binarity, since they show some contribution of the secondary in the spectra, but we can confirm only one of them. We present here an object that can be clearly defined as double line spectroscopic binary or SB2.

On the left-hand side of Fig. 3 we plot a example of the FXCOR cross-correlation were the peak of each component can clearly be seen and so fitted separately. On right-hand side of the Fig. 3, we plot a piece of spectra of our target (below) and the reference single star GI 876 (above). The absorption lines from both components are also well distinguished.

Due to the SB2 nature we could measure the radial and rotational velocity of both components (see Table 4 and Sect. 4). We derived Galactic space-velocity components (U, V, W) in the same way we specify in Sect. 4.

Since we have the double lines in the spectra, when we applied the indexes criteria for obtaining the spectral classification, we have the lines of both components together that we could not disentangle. This produce an uncertainty in the spectral classification an so in the distances derived.

In order to obtain an estimate of the spectral type we use other objects observed in the same run to construct synthetic spectra by using the program STARMOD (see Sect.

4.4). STARMOD allows to rotationally broaden spectra and shift them in the velocity space. We ran it on the spectra of several spectral types objects and combined with the appropriate weights to create composite spectra that were used as template for comparison with our target. The best fit we find corresponds to a M7 primary and at least M7 or later secondary in a 50/50% contribution, but earlier primary is possible and more spectra would be necessary to improve the results with this technique. The two wavelength regions chosen for the fits are plotted in Fig. 4, centred in the first line of Na I doublet ($\lambda\lambda$ 8183, 8195 Å) and centred in ≈8385 Å where there are several Ca I and Fe I lines. The observed spectra of 2MASS0123-3610 is plotted as continuous line and the correspondent synthetic spectra is overplotted as dashed line.

From the different spectral types possible for the primary, we derive the corresponding distances and galactic velocity components. Fig. 5 represent the correspondent position in the YD area in the UV and VW planes. In any case the binary lies inside the YD area and also inside Hyades MG or IC 2391 MG boxes. Taking into account these possible memberships, we estimate the masses of $0.15M_{\odot}$ and $0.09M_{\odot}$ for primary and secondary components respectively if the system belongs to the Hyades MG and $0.06M_{\odot}$ and $0.04M_{\odot}$ if it belongs to the IC 2391 MG.

Rotational velocity measurements give a value at the limit of our sensitivity (≈10 km s^{-1}) for both components. This fact, the binarity and the uncertainty of the spectral classification gives us no clear conclusion about its youth using rotational velocity criterion.

We will take high resolution spectra to follow up the target and measure radial velocities through the period in order to get the orbital parameters. Due to the SB2 nature we will be able to get the masses of both components. If the system is confirmed to belong to Hyades or IC 2391, we will have a presumably coeval UCD system with known age, metallicity and stellar parameters. Identifying such objects is crucial to increase the sample of benchmarks that can provide empirical constraints for star formation theories.

6 CONCLUSIONS AND FUTURE WORK

6.1 Conclusions

We studied the spectra of a 68 target sample of low-mass object previously selected via photometric and astrometric criteria, as possible members to five known young moving group. Using high resolution spectra we measure spectral types and derive distances to determine galactic space-velocity components. After applying kinematic criterion we find that 49 targets belong to the young disk area and that 36 of them possibly belong to one of our five moving groups. We measure when possible projected rotational velocities in order to use the rotation rate as a supporting criterion of youth and so confirm the kinematic members. We find that from the young disk targets, 31 have rotational velocities in agreement with their youth and 12 can not be dismissed as YD due to rotational velocities and further criteria should be applied.

These new candidates significantly increase the known population of low-mass young MG members, which gives rise to an important statistical improvement in calculations of each clusters IMF.

Within the sample, we find a SB2 binary possible member of Hyades or IC 2391 MGs. The spectral type classification gives as a ≈M5-M7 primary and a possible later than M7 secondary. The rotational velocity criterion in this case is not conclusive so further criteria should be applied. Follow up spectroscopy will be carried out in order to improve the classification and to obtain orbital solution and derive physical parameters. If confirmed as a MG member, this object can serve as a very valuable testbed for evolutionary models.

6.2 Future work

Further reliable spectroscopic criteria should be applied to confirm the youth of the candidates found here. The analysis of some age sensitive spectroscopic signatures such as Li I 6708 Å presence an equivalent width, Hα emission (e.g. West et al. 2008) and gravity sensitive features (e.g. Gorlova et al. 2003; McGovern et al. 2004) will provide reliable age constraints for our sample. As we mentioned in Section 3, UVES observing runs include Li I but it is on a very low signal-to-noise region and so no conclusion could be reached. FEROS run included both Hα and Li I region, but although we can see the emission in Hα in nearly all FEROS targets, the signal-to-noise did not allow us to do any equivalent width measurement, and the Li I region is also unusable due to low signal. We are so currently carrying out new spectroscopic observations to study these two important age features. Detailed information of the criteria and how we will use them depending on the spectral type and MG candidature of our sample can be seen in Sect. 4.4.1 and Fig. 9 in Paper I.

To improve the space motion determination and so improve the kinematic criterion, we are also carrying out a parallax program that will allow us to measure more accurate distance.

Discovering planetary systems around young and low-mass objects would be very revealing for the understanding of planet and stellar formation. By studying these systems we will probe the host mass impact on the formation of different kind of planets and test actual theoretical formation models (Laughlin et al. 2004, Kornet & Wolf 2006, Kornet et al. 2006)

Our compiled sample of young MG members will be targeted in the search for lower mass companions by imaging techniques. Their proximity allows the exploration of the faint circumstellar environment at relative small distances from the star and, since substellar companions cool and fade with time, targeting young systems will give higher probability of detection compared to typical older field objects. From the complete sample, our youngest closest MG members (in the IC 2391 or Pleiades MGs) would allow AO to probe to $1M_{J}$ at separations of ∼1AU using for example NACO (Nasmyth Adaptive Optics System (NAOS), Near-Infrared Imager and Spectrograph (CONICA)) at the VLT.

ACKNOWLEDGMENTS

M.C. Gálvez-Ortiz acknowledges financial support from the European Commission in the form of a Marie Curie Intra

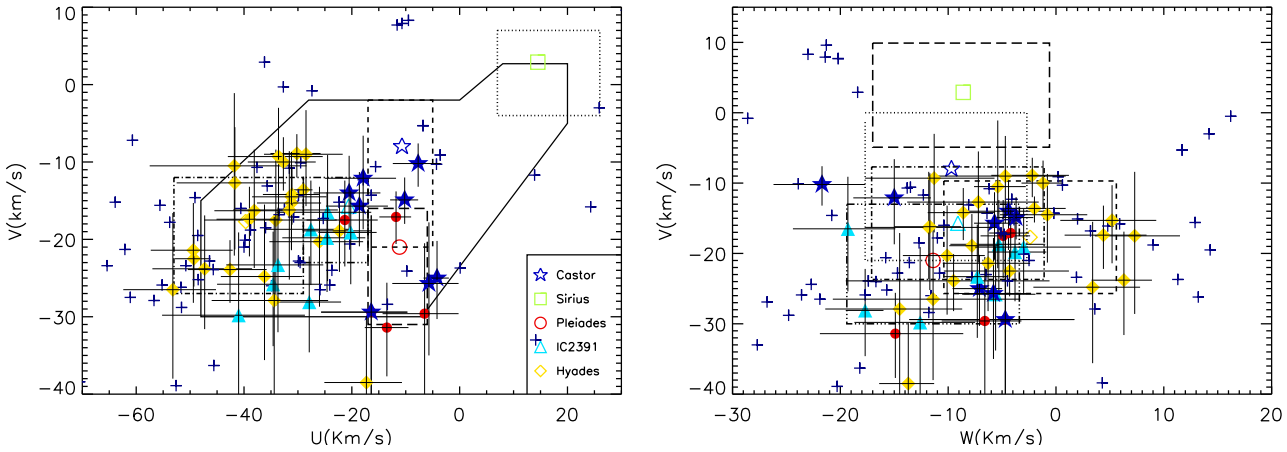

Figure 1. We plot here the UV and VW space motion diagrams for our sample. The young disk boundaries defined by Eggen (1984b,1989) are plot as continuous line. Objects inside these boundaries might be young (YD). The boxes indicate the expected kinematic range for the five MGs. The centre of the 5 main MG are marked (with large open symbols) and our kinematic members are shown as corresponding filled symbols. The objects that are not candidates to be in MGs are plot in crosses. A kinematic member was defined lying inside the relevant box within the uncertainties.

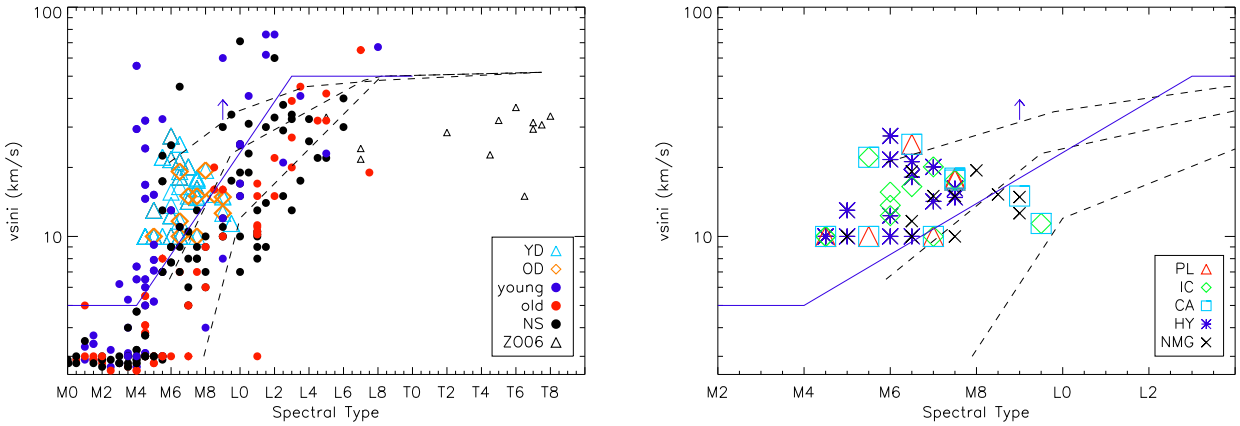

Figure 2. Spectral type versus $v \sin i$. Left: we plot our sample with Reiners & Basri (2008) figure 10 (circles) and open triangles from Zapatero-Osorio et al. (2006). Blue circles are supposed to be young, red circles old and black circles have unknown age. Our data sample is plotted as different symbols depending if they have been classified as YD or OD. As in Reiners & Basri (2008), we mark in dashed lines ages of 2, 5 and 10 Gyr (from upper left to lower right). We plot in blue continuous line the "apparent" separation between the consider "young" and "old" object and so use it as a criterion to determine the possible membership of our targets to the MG they are candidates to. Right: our data sample in the same plot but with different symbols depending of the MG they are a candidate for. The rest of literature data is not plotted here for clarity.

Table 1. Observing runs

Number	Date	Telescope	Instrument	Spect. range (Å)	Orders	Dispersion (Å)	FWHM[1] (Å)
1	28-30/12/06 & 16-17/06/07	ESO-2.2m	FEROS	3500-9200	39	0.033 - 0.081	0.076 - 0.131
2	9/10/-16/12/07	ESO-VLT-U2	UVES	6650-10425	33	0.027-0.041	0.15-0.23
3	23/02-25/02/08	GEMINI	Phoenix	15532-15606	1	0.074	-
4	28/03-21/06/08	ESO-VLT-U2	UVES	6650-10425	33	0.027-0.041	0.15-0.23

[1] Full Width at Half Maximum of the arc comparison lines

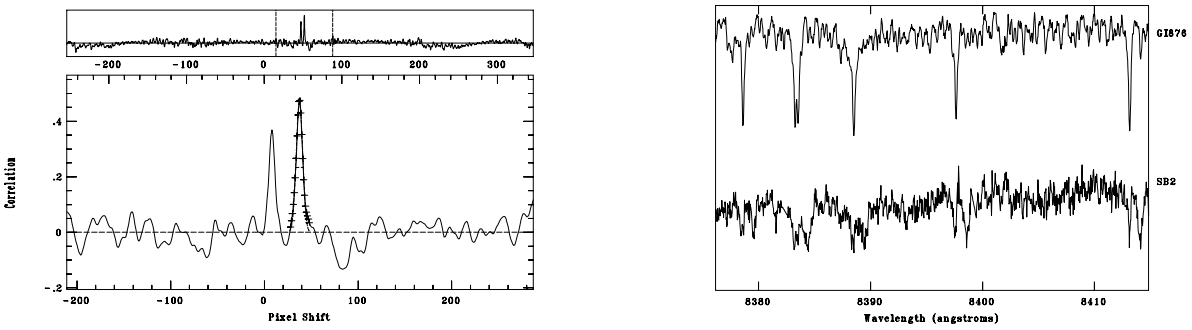

Figure 3. 2MASS0123-3610: On the left side, an example of the FXCOR cross-correlation where the the peak of each component can clearly be seen. On the right side, we plot a piece of spectra of our target (below) and the reference single star GI 876 (above). The absorption lines from both components are also well distinguished.

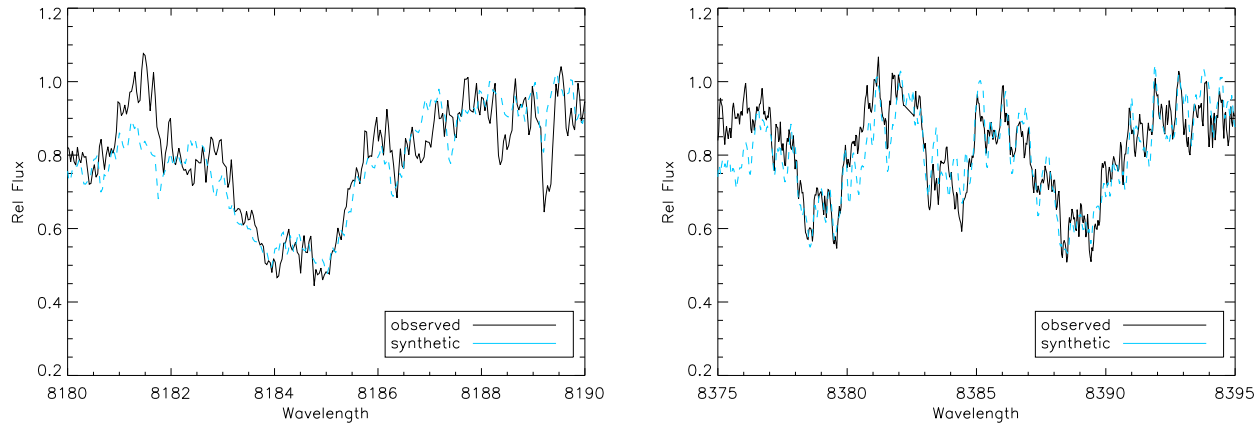

Figure 4. Spectra of 2MASS123-3610 in two different regions, centred in Na I 8183 Å on the left and in 8385 Å on the right. The observed spectrum is plotted as a solid line and the synthetic spectra (made from suitable templates) as a dashed line.

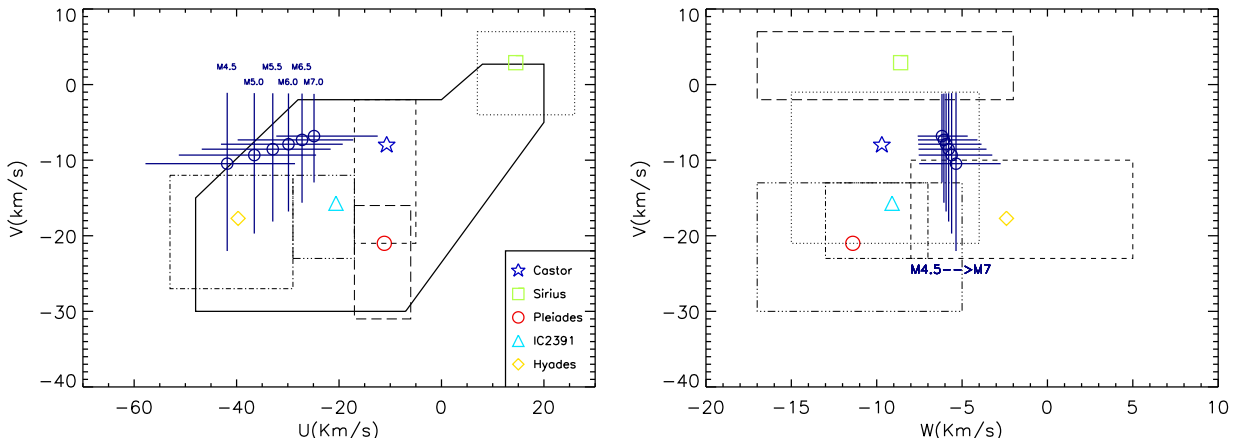

Figure 5. We plot here the UV and VW space motion diagrams for 2MASS0123-3610. The crosses represent the different positions of the system for different (U,V,W) values obtained from the distances derived from spectral type information. All possible positions lie in the YD area and also within the Hyades or IC 2391 boxes.

Table 2. Stellar coordinades, astrometry, spectral types from literature are given with derived spectral types and distances

Name	α (2000) (h m s)	δ (2000) (° ' ")	$\mu_\alpha \cos\delta$ (mas yr^{-1})	μ_δ (mas yr^{-1})	PC3	SpT	SpT (lit)	Distance (pc)	Distance (lit) (pc)
SIPS0004-5721	0 4 18.970	-57 21 23.30	157	-15	1.66	M7.0		45.4±5.5	
SIPS0007-2458	0 7 7.800	-24 58 3.80	192	-59	1.70	M7.0		28.9±3.5	
2MASS0020-2346	0 20 23.155	-23 46 5.38	340	-65	1.43	M6.0		26.4±3.2	
DENIS0021-4244	0 21 5.896	-42 44 43.33	262	-17	2.39	M9.5	M9.5[1]	17.7±2.2	
SIPS0027-5401	0 27 23.240	-54 1 46.20	429	-18	1.47	M6.5	M7.0[2]	25.6±3.1	28±2.5 (Spt)[2]
SIPS0039-2256	0 39 23.250	-22 56 44.90	224	44	1.74	M7.0		47.9±5.8	
DENIS0041-5621	0 41 35.390	-56 21 12.77	92	-62	-	M7.5[3]	M7.5[4]	16.1±2.0	
SIPS0054-4142	0 54 35.300	-41 42 6.20	64	-108	1.25	M5.0		37.9±4.6	
SIPS0109-0343	1 9 51.040	-3 43 26.30	207	87	2.06	M9.0	M9.5[5]	11.0±1.3	9.59±0.2 (plx)[5]
LEHPM1289	1 9 59.579	-24 16 47.82	366	-4	1.47	M6.5		45.2±5.5	
SIPS0115-2715	1 15 26.610	-27 15 54.10	149	32	1.27	M5.5		87.7±10.7	
2MASS0123-3610*	1 23 0.506	-36 10 30.67	124	57	1.19	M5.0		66.1±8.1	
SIPS0126-1946	1 26 49.980	-19 46 5.90	210	-11	1.45	M6.5		62.3±7.6	
LEHPM1563	1 27 31.956	-31 40 3.18	290	131	1.95	M7.0		18.9±2.3	
SIPS0153-5122	1 53 11.430	-51 22 24.99	127	27	1.43	M6.0		44.1±5.4	
2MASS0204-3945	2 4 18.036	-39 45 6.48	119	16	1.66	M7.0		33.9±4.1	
SIPS0212-6049	2 12 33.580	-60 49 18.40	112	-25	1.55	M6.5		36.3±4.4	
SIPS0214-3237	2 14 45.440	-32 37 58.20	148	42	1.49	M6.0		53.2±6.5	
SIPS0235-0711	2 35 49.470	-7 11 21.90	286	75	1.41	M6.0	M5.5[4]	28.2±3.4	
2MASS0334-2130	3 34 10.657	-21 30 34.35	124	7	-	M4.5[3]	M6.0[6]	13.6±4.1	23.3 ±4.0(Spt)[6]
2MASS0429-3123	4 29 18.426	-31 23 56.81	106	69	-	M7.0[3]	M7.5-L0[7] (binary)	9.7±0.9	
SIPS0440-0530	4 40 23.328	-5 30 7.85	330	133	1.74	M7.0	M7.5[2]	9.0±1.1	
2MASS0445-5321	4 45 43.368	-53 21 34.56	343	485	-	M7.5^{phot}		25.5±1.3	
2MASS0502-3227	5 2 38.677	-32 27 50.07	063	-172	1.37	M6	M6.0[6]	29.6±3.6	25.1 ± 3.4(Spt)[6]
2MASS0528-5919	5 28 5.623	-59 19 47.17	77	152	1.34	M6		82.0±10.0	
2MASS0600-3314	6 0 33.750	-33 14 26.84	-28	153	-	M7.0^{phot}	M7.5[6]	33.4±2.6	28.0 ± 2.7(Spt)[6]
SIPS1039-4110	10 39 18.340	-41 10 32.00	25	-173	-	M6.5^{phot}	M6.0[8]	20.8±5.3	
SIPS1124-2019	11 24 22.229	-20 19 1.50	129	-19	-	M7.0^{phot}		37.5±2.5	
DENIS1250-2121	12 50 52.654	-21 21 13.67	457	-320	-	M7.5[3]	M7.5[2]	9.8±0.4	11.1 ± 1.3(Spt)[2]
SIPS1329-4147	13 29 0.872	-41 47 11.90	293	-302	-	M9.5^{phot}	M9.0[8]	27.3±2.4	
SIPS1341-3052	13 41 11.561	-30 52 49.60	109	-163	-	L0^{phot}		40.8±11.5	
2MASS1507-2000	15 7 27.799	-20 0 43.18	114	-76	-	M7.5[3]	M7.5[6]	15.2±0.8	11.0 ± 0.2(Spt)[6]
SIPS1632-0631	16 32 58.799	-6 31 45.30	29	-366	1.95	M8.5	M7.0[8]	19.7±2.4	
SIPS1758-6811	17 58 59.663	-68 11 10.50	3	-182	1.25	M5.5		71.4±8.7	
SIPS1949-7136	19 49 45.527	-71 36 50.89	36	-183	1.59	M7.0		46.2±5.6	
SIPS2000-7523	20 0 48.171	-75 23 6.58	179	-85	1.88	M8.0		20.9±2.5	
2MASS2001-5949	20 1 24.639	-59 49 0.09	163	-54	1.46	M6.0		38.6±4.7	
SIPS2014-2016	20 14 3.523	-20 16 21.30	248	-112	1.71	M7.5	M7.5[6]	22.0±2.7	
2MASS2031-5041	20 31 27.495	-50 41 13.49	161	-160	1.31	M5.5		48.3±5.9	
SIPS2039-1126	20 39 13.081	-11 26 52.30	64	-105	1.61	M7.0	M8.0[6]	42.6±5.2	
SIPS2045-6332	20 45 2.278	-63 32 5.30	97	-201	2.16	M8.5		15.3±1.9	
SIPS2049-1716	20 49 52.610	-17 16 7.80	369	-142	-	M6.5[3]	M6.0[9]	13.2±1.6	
SIPS2049-1944	20 49 19.673	-19 44 31.30	179	-279	1.60	M7.0	M7.5[10]	28.1±3.4	
SIPS2100-6255	21 0 30.227	-62 55 7.31	65	-110	1.19	M5.0	M5.0^{phot}	66.1±10.2	
2MASS2106-4044	21 6 20.896	-40 44 51.91	150	-83	1.47	M6.0		38.8±4.7	
SIPS2114-4339	21 14 40.928	-43 39 51.20	49	-148	1.57	M6.5		31.1±3.8	
SIPS2119-0740	21 19 17.571	-7 40 52.50	152	-117	1.64	M7.0		47.0±5.7	
HB2124-4228	21 27 26.133	-42 15 18.39	97	-170	1.76	M8.0	M8.5[11]	29.9±3.6	35.7±10.1(plx)[12]
SIPS2128-3254	21 28 17.402	-32 54 3.90	338	-166	-	M6.5[3]		33.0±1.0	
DENIS2200-3038	22 0 2.022	-30 38 32.71	199	-66	2.07	M9.0	M9-L0[13]	24.8±3.0	35 ± 2(Spt[13])
SIPS2200-2756	22 0 16.838	-27 56 29.70	156	-8	1.46	M6.0		35.5±4.4	
2MASS2207-6917	22 7 10.313	-69 17 14.25	131	-51	1.49	M6.5		43.2±5.3	
LEHPM4480	22 15 10.151	-67 38 49.07	260	-136	1.33	M6.0		51.9±6.3	
2MASS2222-4919	22 22 3.684	-49 19 23.45	67	-122	1.38	M6.0		76.9±9.4	
2MASS2231-4443	22 31 8.657	-44 43 18.43	163	-9	1.23	M5.0		46.3±5.6	
LEHPM4908	22 36 42.656	-69 34 59.30	220	-63	1.39	M6.0		32.3±3.9	
2MASS2242-2659	22 42 41.294	-26 59 27.23	99	-26	1.33	M5.5		47.4±5.8	
2MASS2254-3228	22 54 58.110	-32 28 52.20	55	-84	1.37	M6.0		49.7±6.1	
2MASS2311-5256	23 11 30.330	-52 56 30.17	141	-43	1.36	M5.5		66.5±8.1	
SIPS2318-4919	23 18 45.952	-49 19 17.79	227	-25	-	M7.0^{phot}	M8.0[2]	48.9±3.7	
SIPS2321-6106	23 21 43.418	-61 6 35.37	110	58	1.31	M5.5		49.5±6.0	
SIPS2322-6357	23 22 5.332	-63 57 57.60	122	-28	1.54	M6.5	M7.0[2]	56.4±6.9	
SIPS2341-3550	23 41 47.497	-35 50 14.40	154	-28	1.64	M7.0		36.7±4.5	
SIPS2343-2947	23 43 34.731	-29 47 9.50	257	-8	1.83	M8.0		32.3±3.9	
SIPS2347-1821	23 47 16.662	-18 21 50.60	219	41	1.57	M6.5		31.8±3.9	
SIPS2350-6915	23 50 3.948	-69 15 24.39	164	11	1.52	M6.0		56.1±6.8	
LEHPM6375	23 52 49.138	-22 49 29.54	222	-175	1.51	M6.0		33.0±4.0	
LEHPM6542	23 57 54.822	-19 55 1.89	185	-4	1.41	M6.0		42.3±5.2	

[1] Basri et al. 2000, ApJ, 538, 363. [2] Lodieu et al. 2005, A&A 440, 1061. [3] Feros run object. See Sect 4.1 and Paper I. [4] Phan-Bao & Bessel, 2006, A&A, 446, 51. [5] Costa et al, 2005, AJ, 130, 337. [6] Cruz et al. 2003, AJ, 126, 2421. [7] Siegler et al., 2005,621, 1023. [8] Gizis, 2002, ApJ, 575, 484. [9] Crifo et al., 2005, A&A 441, 653. [10] Basri & Reiners, 2006, AJ, 132, 663. [11] Burgasser et al., 2002, ApJ, 564, 421. [12] Tinney, 1996, MNRAS, 281, 644. [13] Burgasser, 2006, AJ, 131, 1007. ^{phot} Spectral types derived by J-I colors. See text. '*' See Sect. 5.3

Table 3. Radial and Rotational are given for our reference stars

Name	SpT	V_r (km s^{-1})	Ref$_{V_r}$	$V \sin i$ (km s^{-1})	Ref$_{V \sin i}$	Observing run
GI 876	M4.0	-1.591	[1]	<2.0	[2]	1,2,4
GL 406	M6.0	-19.402	[1]	<3.0	[2]	1,3
VB 10	M8.0	34.7	[3]	6.5	[2]	1,4
GJ 3877	M7.0	1.4	[2]	8.0	[2]	1
LP 944-20	M9.0	10	[4]	30.3	[5]	1,2,3

[1] Nidever et al., 2002, ApJ, 141, 503
[2] Mohanty, 2003, ApJ, 583, 451
[3] Martín et al., 2006, ApJ, 644, L75
[4] Ribas 2003, A&A, 398, 239R
[5] Zapatero-Osorio et al, 2006, AJ, 647, 1405

European Fellowship (PIEF-GA-2008-220679). Based on observations made with ESO Telescopes, with FEROS echelle spectrometer mounted on the 2.2-m telescope based at La Silla (Chile) under programmes 078.C-0333(A) and 079.C-0255(A), and with UVES high-resolution optical spectrograph at VLT Kueyen 8.2-m telescope at Paranal (chile) in programmes 079.C-0308(A), 080.C-0923(A) and 081.C-0222(A). And Observations obtained at the Gemini Observatory, which is operated by the Association of Universities for Research in Astronomy, Inc., under a cooperative agreement with the NSF on behalf of the Gemini partnership: the National Science Foundation (United States), the Science and Technology Facilities Council (United Kingdom), the National Research Council (Canada), CONICYT (Chile), the Australian Research Council (Australia), Ministrio da Cincia e Tecnologia (Brazil) and Ministerio de Ciencia, Tecnologa e Innovacin Productiva (Argentina), with the Phoenix infrared spectrograph, developed and operated by the National Optical Astronomy Observatory in program GS-2008A-C-1.

REFERENCES

Ahmic M., Jayawardhana R., Brandeker A., Scholz A., van Kerkwijk M. H., Delgado-Donate E., Froebrich D., 2007, ApJ, 671, 2074
Antoja T., Figueras F., Fernández D., Torra J., 2008, A&A, 490, 135A
Bailer-Jones C. A. L., 2004, A&A, 419, 703
Barrado Y Navacués D., 1998, A&A, 339, 891
Barrado Y Navacués D., Stauffer J. R., Patten B. M., 1999, ApJ, 522, L53
Barrado Y Navacués D., Stauffer J. R., Jayawardhana J., 2004, AJ, 614, 386
Baraffe I., Chabrier G., Allard F., Hauschildt P. H., 1998, A&A, 337, 403
Basri G., Mohanty S., Allard F., Hauschildt P. H., Delfosse X., Martín E. L., Forveille T., Goldman B., 2000, ApJ, 538, 363
Basri G., Reiners A., 2006, AJ, 132, 663
Barden S. C., 1985, ApJ, 295, 162
Bouvier J., Kendall T., Meeus G., Testi L., Moraux E., Stauffer J. R., James D., Cuillandre J. C., Irwin J., McCaughrean M. J., Baraffe I., Bertin E., A&A, 481, 661B
Burgasser A. J., Kirkpatrick J. D, Brown M. E., Reid I. N., Burrows A., Liebert J. et al., 2002, ApJ, 564, 421
Burgasser A. J., Burrows A., Kirkpatrick J. D, 2006, ApJ, 639, 1095
Burningham B., Leggett S. K., Lucas P. W., Pinfield D. J., Smart R. L., Day-Jones A. C., Jones H. R. A., Murray D., Nickson E., Tamura M., Zhang Z., Lodieu N., Tinney C. G., Zapatero Osorio M. R., 2010, MNRAS, arXiv:1001.4393v1
Caballero J. A., 2010, A&A, 2010arXiv1001.5432C
Clarke J. R. A., Pinfield D. J., Gálvez-Ortiz M. C., Jenkins J. S., Burningham B., Deacon N. R., Jones H. R. A., Pokorny, R. S., Barnes J. R., Day-Jones A. C., 2010, MNRAS, 402, 575
Close L. M., Siegler N., Freed M., Biller B., 2003, ApJ, 587, 407
Close L. M., Zuckerman B., Song I., Barman T., Marois C., Rice E.L., Siegler N., Macintosh B., Becklin E. E., Campbell R., Lyke J. E., Conrad A., Le Mignant D., 2007, ApJ, 660, 1492
Costa E., Méndez R. A., Jao W. C., Henry T. J., Subasavage J. P., Brown M. A., Ianna P. A., Bartlett J., 2005, AJ, 130, 337
Crifo F., Phan-bao N., Delfosse X., Forveille T., Guilbert J., Martín E.L., Reylé C., 2005, A&A, 441, 653
Cruz K. L., Reid I. N., 2002, AJ, 123, 2828
Cruz K. L., Reid I. N., Liebert J., Kirkpatrick J. D., Lowrance P. J., 2003, AJ, 126, 2421
Dehnen W., 1998, AJ, 115, 2384
Dahn C. C., Harris H. C., Vrba F. J., Guetter H. H., Canzian B., Henden A. A., Levine S. E., Luginbuhl C. B. et al. 2002, AJ, 124, 1170
Day-Jones A. C., Pinfield D. J., Napiwotzki R., Burningham B., Jenkins J. S., Jones H. R. A., Folkes S. L., Weights D. J., Clarke J. R. A., 2008, MNRAS, 388, 838
Dekker H., D'Odorico S., Kaufer A., Delabre B., Kotzlowski H., 2000, SPIE, 4008, 534.
De Simone R., Xiaoan W., Tremaine S., 2004, MNRAS, 350, 627D
Dobbie P. D., Pineld D. J., Jameson R. F., Hodgkin S. T., 2002, MNRAS, 335, L79
Duquennoy A., Mayor M., 1991, A&A, 248, 485
Dupuy T. J., Liu M. C., Ireland M. J., 2009a, AJ, 692, 729
Dupuy T. J., Liu M. C., Ireland M. J., 2009b, ApJ, 699, 168
Eggen O. J., 1983, MNRAS 204, 391

Table 4. MG assignment are given based on galactic velocity coordinates. (-) indicates values not measured due to the low signal-to-noise of the spectra.

Name	$V_r \pm \sigma_{V_r}$ (km s^{-1})	distance (pc)	$U \pm \sigma_U$ (km s^{-1})	$V \pm \sigma_V$ (km s^{-1})	$W \pm \sigma_W$ (km s^{-1})	MG candidature	$V \sin i$ (km s^{-1})	Observing run	S/N
SIPS0004-5721	6.54±0.46	69.3 ± 8.5	$-41.0^{+12.3}_{-14.2}$	$-29.8^{+10.7}_{-12.8}$	$-12.6^{+5.1}_{-6.1}$	**IC 2391**	20.11	2	22
”		45.4 ± 5.5	$-26.0^{+8.1}_{-9.3}$	$-20.3^{+7.1}_{-8.4}$	$-10.1^{+3.5}_{-4.1}$	**Hyades**			
”		51.6 ± 6.3	$-29.9^{+9.2}_{-10.6}$	$-22.8^{+8.0}_{-9.5}$	$-10.8^{+3.9}_{-4.7}$	Castor			
SIPS0007-2458	10.43±0.46	38.0 ± 4.6	$-23.7^{+5.1}_{-5.6}$	$-24.0^{+5.1}_{-5.6}$	$-16.7^{+1.5}_{-1.6}$	Pleiades	17.96	2	24
”		44.2 ± 5.4	$-27.9^{+5.9}_{-6.5}$	$-28.1^{+5.9}_{-6.5}$	$-17.7^{+1.7}_{-1.8}$	**IC 2391**			
”		32.9 ± 4.0	$-20.4^{+4.4}_{-4.9}$	$-20.6^{+4.4}_{-4.9}$	$-15.8^{+1.4}_{-1.5}$	Castor			
2MASS0020-2346	2.19±0.15	40.3 ± 4.9	$-49.9^{+9.4}_{-10.3}$	$-42.2^{+8.5}_{-9.4}$	$-10.8^{+1.6}_{-1.7}$	IC 2391	12.32	4	24
DENIS0021-4244	2.00±3.00	27.1 ± 3.3	$-27.1^{+7.0}_{-8.0}$	$-19.0^{+5.8}_{-6.8}$	$-7.5^{+1.8}_{-2.1}$	**IC 2391**	11.39	2	20
”		17.7 ± 2.2	$-17.4^{+4.6}_{-5.3}$	$-12.7^{+3.8}_{-4.5}$	$-6.3^{+1.3}_{-1.5}$	Hyades			
”		20.2 ± 2.5	$-19.9^{+5.2}_{-6.0}$	$-14.4^{+4.3}_{-5.1}$	$-6.6^{+1.4}_{-1.6}$	**Castor**			
SIPS0027-5401	-11.49±0.88	39.1 ± 4.8	$-70.5^{+13.3}_{-14.6}$	$-38.4^{+10.4}_{-11.7}$	$4.3^{+3.6}_{-4.1}$	IC 2391	27.43	4	22
”		25.6 ± 3.1	$-47.3^{+8.8}_{-9.7}$	$-23.8^{+6.9}_{-7.8}$	$6.3^{+2.6}_{-3.0}$	**Hyades**			
SIPS0039-2256	-16.04±0.26	47.9 ± 5.8	$-48.6^{+10.7}_{-12.0}$	$-19.5^{+7.0}_{-8.3}$	$14.3^{+0.9}_{-1.0}$	Hyades	12.82	2	20
DENIS0041-5621	2.36±1.03	18.3 ± 2.2	$-3.7^{+2.3}_{-2.7}$	$-9.2^{+2.9}_{-3.3}$	$0.3^{+2.0}_{-1.8}$	Sirius	≈15[1]	1	21
”		21.1 ± 2.6	$-4.4^{+2.6}_{-3.0}$	$-10.4^{+3.3}_{-3.7}$	$0.6^{+2.1}_{-1.9}$	Pleiades			
”		18.3 ± 2.2	$-3.7^{+2.3}_{-2.7}$	$-9.2^{+2.9}_{-3.3}$	$0.3^{+2.0}_{-1.8}$	Castor			
SIPS0054-4142	-5.81±0.25	43.1 ± 5.3	$0.1^{+3.5}_{-3.3}$	$-23.7^{+5.7}_{-6.4}$	$11.3^{+1.6}_{-1.4}$	Castor	<10	4	26
LEHPM1289	23.36±0.10	45.2 ± 5.5	$-65.6^{+14.3}_{-16.1}$	$-45.6^{+12.2}_{-14.0}$	$-17.7^{+1.5}_{-1.4}$	Hyades	12.62	2	26
SIPS0109-0343	-10.36±0.64	9.6 ± 0.2	$-6.8^{+3.5}_{-3.6}$	$-5.3^{+3.4}_{-3.5}$	$11.7^{+1.8}_{-1.7}$	Hyades		4	27
SIPS0115-2715	43.51±0.12	87.7 ± 10.7	$-61.1^{+11.4}_{-12.6}$	$-27.5^{+7.4}_{-8.6}$	$-37.6^{+1.2}_{-1.1}$	Hyades	<10	2	20
2MASS0123-3610*	7.53±0.29*	101.0 ± 12.3	$-63.9^{+15.5}_{-24.0}$	$-15.2^{+14.3}_{-17.6}$	$-4.3^{+3.8}_{-3.1}$	IC 2391	<10/<10	2	24
”		66.1 ± 8.1	$-41.8^{+13.4}_{-15.7}$	$-10.5^{+9.4}_{-11.6}$	$-5.4^{+2.6}_{-2.2}$	**Hyades**			
SIPS0126-1946	28.89±0.14	62.23 ± 7.6	$-52.6^{+17.6}_{-20.9}$	$-38.9^{+16.9}_{-20.2}$	$-20.3^{+4.1}_{-3.4}$	Hyades	>13[1]	2	19
LEHPM1563	27±0.25	18.9 ± 2.3	$-29.5^{+5.0}_{-5.5}$	$-10.1^{+2.5}_{-2.9}$	$-23.9^{+0.9}_{-0.8}$	Hyades	15.25	2	27
SIPS0153-5122	1.35±0.24	57.8 ± 7.1	$-29.6^{+7.8}_{-9.0}$	$-23.0^{+5.8}_{-6.9}$	$-6.5^{+3.2}_{-2.7}$	Pleiades	13.67	2	22
”		67.3 ± 8.2	$-34.6^{+9.1}_{-10.4}$	$-25.8^{+6.8}_{-8.0}$	$-5.6^{+3.7}_{-3.1}$	**IC 2391**			
”		44.1 ± 5.4	$-22.3^{+6.0}_{-6.8}$	$-18.9^{+4.5}_{-5.3}$	$-7.8^{+2.5}_{-2.1}$	**Hyades**			
2MASS0204-3945	11.90±0.13	44.5 ± 5.4	$-21.3^{+6.1}_{-7.1}$	$-17.5^{+5.1}_{-6.0}$	$-4.9^{+2.5}_{-2.1}$	**Pleiades**	<10	2	22
”		51.8 ± 6.3	$-24.6^{+7.1}_{-8.3}$	$-19.8^{+5.9}_{-7.0}$	$-3.8^{+2.9}_{-2.5}$	**IC 2391**			
”		33.9 ± 4.1	$-16.4^{+4.7}_{-5.4}$	$-14.3^{+3.9}_{-4.6}$	$-6.4^{+1.9}_{-1.7}$	Hyades			
”		38.6 ± 4.7	$-18.6^{+5.3}_{-6.2}$	$-15.7^{+4.4}_{-5.2}$	$-5.7^{+2.2}_{-1.9}$	**Castor**			
SIPS0212-6049	13.11±0.15	41.3 ± 5.0	$-9.8^{+3.5}_{-4.1}$	$-24.1^{+3.8}_{-4.3}$	$-1.3^{+2.8}_{-2.4}$	Sirius	<10	2	23
SIPS0214-3237	4.01±0.37	81.3 ± 9.9	$-51.7^{+17.2}_{-20.3}$	$-26.2^{+13.9}_{-16.9}$	$13.2^{+6.3}_{-5.4}$	IC 2391	18.14	2	22
”		53.2 ± 6.5	$-34.1^{+11.3}_{-13.3}$	$-17.5^{+9.1}_{-11.1}$	$7.3^{+4.2}_{-3.7}$	**Hyades**			
SIPS0235-0711	16.61±31	28.2 ± 3.4	$-39.0^{+5.6}_{-6.1}$	$-17.4^{+4.2}_{-4.8}$	$4.4^{+4.0}_{-3.6}$	**Hyades**	21.65	4	32
2MASS0334-2130	18.98±0.80	20.7 ± 6.3	$-15.9^{+3.5}_{-4.5}$	$-13.9^{+3.9}_{-5.0}$	$-7.9^{+4.2}_{-3.5}$	**IC 2391**	<10[1]	1	26
2MASS0429-3123	41.92±0.88	14.8 ± 1.4	$-25.2^{+2.2}_{-2.5}$	$-26.3^{+1.9}_{-2.2}$	$-22.5^{+2.2}_{-2.0}$	IC 2391	<10[1]	1	26
”		11.0 ± 1.0	$-23.7^{+1.7}_{-1.9}$	$-25.8^{+1.6}_{-1.7}$	$-24.0^{+1.8}_{-1.7}$	Castor			
SIPS0440-0530	28.28±0.32	10.2 ± 1.2	$-29.9^{+1.92.1}$	$-14.3^{+1.9}_{-2.3}$	$-0.2^{+3.3}_{-3.0}$	Sirius	14.79	2	31
”		11.8 ± 1.4	$-31.0^{+2.2}_{-2.4}$	$-15.1^{+2.2}_{-2.6}$	$2.0^{+3.8}_{-3.4}$	Pleiades			
”		13.7 ± 1.7	$-32.5^{+2.5}_{-2.7}$	$-16.1^{+2.6}_{-3.0}$	$4.8^{+4.4}_{-4.0}$	IC 2391			
”		9.0 ± 1.1	$-29.0^{+1.7}_{-1.9}$	$-13.6^{+1.7}_{-2.0}$	$-2.0^{+2.9}_{-2.7}$	**Hyades**			
”		10.2 ± 1.2	$-29.9^{+1.9}_{-2.1}$	$-14.3^{+1.9}_{-2.3}$	$-0.2^{+3.3}_{-3.0}$	Castor			
2MASS0445-5321	68.46±1.14	25.5 ± 1.3	$-74.1^{+4.8}_{-5.0}$	$-63.4^{+2.3}_{-2.4}$	$-18.4^{+3.0}_{-2.9}$	Hyades	-	3	14
2MASS0502-3227	-4.33±0.15	33.7 ± 4.1	$24.3^{+5.4}_{-4.8}$	$-15.8^{+4.6}_{-5.2}$	$5.9^{+3.1}_{-2.6}$	Sirius	12.28	4	22
2MASS0528-5919	-6.81±0.48	82.0 ± 10.0	$-60.7^{+15.5}_{-17.8}$	$-7.2^{+6.0}_{-7.1}$	$26.3^{+10.3}_{-8.7}$	Hyades	<10	2	17
2MASS0600-3314	35.36±5.00	33.4 ± 2.6	$-38.1^{+6.9}_{-7.4}$	$-16.3^{+7.9}_{-7.4}$	$-11.8^{+6.3}_{-5.9}$	**Hyades**	-	3	18
SIPS1039-4110	9.98±5.00	23.7 ± 6.0	$13.9^{+5.0}_{-4.5}$	$-11.7^{+5.6}_{-5.7}$	$-12.3^{+5.7}_{-6.1}$	Sirius	-	3	15
SIPS1124-2019	13.51±5.00	57.3 ± 3.8	$34.3^{+10.1}_{-9.2}$	$-0.5^{+9.4}_{-8.8}$	$16.2^{+9.4}_{-8.7}$	IC 2391	-	3	19
”		42.7 ± 2.8	$25.9^{+7.6}_{-7.0}$	$-3.0^{+8.0}_{-7.5}$	$14.2^{+7.8}_{-7.2}$	Castor			
DENIS1250-2121	-7.59±0.38	12.8 ± 0.6	$27.3^{+2.8}_{-2.7}$	$9.0^{+1.6}_{-1.5}$	$-19.5^{+1.6}_{-1.7}$	Pleiades	-	1	33
SIPS1329-4147	34.15±5.00	35.8 ± 3.2	$65.3^{+9.8}_{-9.4}$	$-13.3^{+7.6}_{-7.1}$	$-42.6^{+9.4}_{-10.0}$	Pleiades	-	3	13
SIPS1341-3052	33.68±5.00	46.5 ± 13.0	$46.1^{+14.5}_{-10.6}$	$-23.9^{+7.0}_{-9.0}$	$-17.4^{+14.8}_{-16.8}$	Sirius	-	3	20
”		53.6 ± 15.0	$50.0^{+16.2}_{-14.1}$	$-24.4^{+7.6}_{-9.9}$	$-22.7^{+16.7}_{-19.0}$	Pleiades			
”		46.5 ± 13.0	$46.1^{+14.5}_{-12.6}$	$-23.9^{+7.0}_{-9.0}$	$-17.4^{+14.8}_{-16.8}$	Castor			
2MASS1507-2000	-22.10±1.33	17.3 ± 0.9	$-11.2^{+2.4}_{-2.3}$	$7.8^{+2.3}_{-2.1}$	$-20.8^{+2.6}_{-2.8}$	Sirius	-	1	20
”		19.9 ± 1.0	$-10.1^{+2.6}_{-2.5}$	$8.1^{+2.6}_{-2.3}$	$-22.2^{+2.9}_{-3.1}$	Pleiades			
”		23.2 ± 1.2	$-8.9^{+2.9}_{-2.8}$	$8.4^{+2.9}_{-2.7}$	$-23.8^{+3.2}_{-3.5}$	IC 2391			
”		17.3 ± 0.9	$-11.2^{+2.4}_{-2.3}$	$7.8^{+2.3}_{-2.1}$	$-20.8^{+2.6}_{-2.8}$	Castor			

Table 4 – *continued*

Name	$V_r \pm \sigma_{V_r}$ (km s^{-1})	distance (pc)	$U \pm \sigma_U$ (km s^{-1})	$V \pm \sigma_V$ (km s^{-1})	$W \pm \sigma_W$ (km s^{-1})	MG candidature	$V \sin i$ (km s^{-1})	Observing run	S/N
SIPS1632-0631	-4.76±0.54	25.9 ± 3.2	$14.1^{+5.1}_{-4.6}$	$-33.0^{+8.0}_{-9.0}$	$-27.7^{+6.9}_{-7.8}$	Pleiades	15.23	4	23
SIPS1758-6811	45.90±0.27	71.4 ± 8.7	$-3.5^{+7.0}_{-7.5}$	$-66.2^{+8.7}_{-9.7}$	$-38.9^{+6.5}_{-7.5}$	Hyades	10.40	4	22
SIPS1949-7136	28.69±0.25	60.7 ± 7.4	$-14.1^{+9.0}_{-10.3}$	$-55.8^{+10.1}_{-11.4}$	$-19.7^{+5.1}_{-6.3}$	Pleiades	-	4	20
”		70.6 ± 8.6	$-19.7^{+10.5}_{-12.0}$	$-62.5^{+11.7}_{-13.3}$	$-20.6^{+5.9}_{-7.3}$	IC 2391			
”		46.2 ± 5.6	$-6.0^{+6.9}_{-7.9}$	$-46.0^{+7.7}_{-8.7}$	$-18.5^{+3.9}_{-4.8}$	Hyades			
SIPS2000-7523	11.77±0.97	23.7 ± 2.9	$-7.7^{+4.2}_{-4.7}$	$-10.2^{+2.6}_{-3.0}$	$-21.7^{+4.0}_{-4.5}$	**Castor**	-	4	22
2MASS2001-5949	-19.58±0.53	43.9 ± 5.4	$-36.2^{+6.1}_{-7.0}$	$2.9^{+5.1}_{-6.0}$	$-18.4^{+6.8}_{-7.6}$	Castor	19.10	4	20
SIPS2014-2016	-46.29±0.45	33.6 ± 4.1	$-55.2^{+4.6}_{-5.2}$	$-25.9^{+4.5}_{-5.4}$	$-17.7^{+8.2}_{-9.1}$	IC 2391	16.18	4	22
”		22.0 ± 2.7	$-49.3^{+3.1}_{-3.5}$	$-22.5^{+3.0}_{-3.6}$	$-4.3^{+5.5}_{-6.1}$	**Hyades**			
”		25.0 ± 3.1	$-50.8^{+3.9}_{-4.0}$	$-23.4^{+3.4}_{-4.0}$	$-7.8^{+6.2}_{-6.9}$	Castor			
2MASS2031-5041	-30.93±0.50	48.3 ± 5.9	$-53.2^{+8.0}_{-9.2}$	$-26.5^{+9.9}_{-11.5}$	$-11.4^{+8.1}_{-9.3}$	**Hyades**	13.00	4	19
SIPS2039-1126	-18.01±2.00	56.0 ± 6.8	$-13.5^{+4.0}_{-4.1}$	$-31.4^{+5.8}_{-6.3}$	$-14.9^{+6.3}_{-7.0}$	**Pleiades**	>15	4	20
”		48.5 ± 5.9	$-13.4^{+3.6}_{-3.7}$	$-28.4^{+5.1}_{-5.6}$	$-11.8^{+5.6}_{-6.2}$	Castor			
SIPS2045-6332	0.53±0.53	20.0 ± 2.4	$-11.8^{+2.8}_{-3.1}$	$-17.1^{+3.3}_{-3.5}$	$-4.2^{+1.7}_{-2.0}$	**Pleiades**	>15	4	29
”		17.4 ± 2.1	$-10.2^{+2.5}_{-2.7}$	$-14.9^{+2.9}_{-3.1}$	$-3.7^{+1.6}_{-1.8}$	**Castor**			
SIPS2049-1716	-35.38±2.40	20.1 ± 2.4	$-44.0^{+6.5}_{-7.2}$	$-24.6^{+3.6}_{-4.0}$	$-11.7^{+8.2}_{-9.0}$	IC 2391	-	1	17
”		13.2 ± 1.6	$-37.6^{+4.8}_{-5.3}$	$-21.1^{+2.7}_{-3.0}$	$-0.9^{+5.8}_{-6.4}$	**Hyades**			
SIPS2049-1944	1.62±1.00	36.9 ± 4.5	$-6.3^{+2.7}_{-3.0}$	$-42.6^{+6.8}_{-7.2}$	$-38.9^{+6.5}_{-6.8}$	Pleiades	18.71	4	31
SIPS2100-6255	-18.23±0.41	66.1 ± 10.2	$-36.2^{+7.0}_{-8.1}$	$-24.8^{+9.3}_{-10.8}$	$3.4^{+4.4}_{-5.5}$	**Hyades**	-	4	10
2MASS2106-4044	-50.05±0.38	59.3 ± 7.2	$-65.4^{+7.7}_{-8.9}$	$-23.4^{+9.4}_{-11.3}$	$1.9^{+8.7}_{-10.0}$	IC 2391	22.12	4	21
”		38.8 ± 4.7	$-55.6^{+5.2}_{-5.9}$	$-15.6^{+6.2}_{-7.4}$	$12.9^{+5.8}_{-6.6}$	Hyades			
SIPS2114-4339	2.69±0.25	35.4 ± 4.3	$-4.2^{+2.2}_{-2.5}$	$-25.0^{+4.8}_{-5.3}$	$-7.1^{+2.1}_{-2.5}$	**Castor**	25.22	4	18
SIPS2119-0740	-45.50±0.34	61.7 ± 7.5	$-43.7^{+5.3}_{-6.2}$	$-54.8^{+6.1}_{-6.7}$	$-17.8^{+8.6}_{-9.4}$	Pleiades	16.35	4	17
”		71.9 ± 8.8	$-46.5^{+6.2}_{-7.2}$	$-59.6^{+7.1}_{-7.8}$	$-25.1^{+10.0}_{-11.0}$	IC 2391			
HB2124-4228	-7.64±0.33	35.7 ± 10.1	$-16.4^{+6.7}_{-9.3}$	$-29.4^{+12.5}_{-15.7}$	$-4.7^{+6.4}_{-8.9}$	**Pleiades**	17.61	4	20
SIPS2128-3254	-19.77±2.15	33.0 ± 1.0	$-48.0^{+4.5}_{-4.6}$	$-31.1^{+3.5}_{-3.7}$	$-24.2^{+4.5}_{-4.6}$	Hyades	≈ 13[1]	1	24
DENIS2200-3038	-25.00±0.14	37.9 ± 4.6	$-40.0^{+8.3}_{-9.8}$	$-21.0^{+7.7}_{-9.2}$	$-2.5^{+6.3}_{-7.2}$	IC 2391	14.86	4	30
”		24.8 ± 3.0	$-31.2^{+5.5}_{-6.4}$	$-15.3^{+5.0}_{-6.1}$	$5.2^{+4.1}_{-4.8}$	**Hyades**			
”		28.2 ± 3.4	$-33.5^{+6.2}_{-7.3}$	$-16.8^{+5.7}_{-6.9}$	$3.2^{+4.7}_{-5.4}$	Castor			
SIPS2200-2756	-17.43±0.34	35.5 ± 4.4	$-30.2^{+4.4}_{-4.9}$	$-8.9^{+2.5}_{-3.1}$	$-2.2^{+3.4}_{-3.8}$	**Hyades**	<10	4	22
2MASS2207-6917	-9.21±0.41	56.6 ± 6.9	$-35.7^{+8.8}_{-10.1}$	$-13.1^{+7.4}_{-8.8}$	$-8.1^{+7.3}_{-8.7}$	Pleiades	11.66	4	22
”		65.9 ± 8.0	$-40.6^{+10.2}_{-11.8}$	$-16.0^{+8.6}_{-10.2}$	$-10.4^{+8.4}_{-10.1}$	IC 2391			
”		43.2 ± 5.3	$-28.5^{+6.8}_{-7.8}$	$-9.0^{+5.7}_{-6.7}$	$-4.7^{+5.6}_{-6.7}$	**Hyades**			
”		49.1 ± 6.0	$-31.6^{+7.7}_{-8.8}$	$-10.8^{+6.4}_{-7.6}$	$-6.2^{+6.3}_{-7.6}$	Castor			
LEHPM4480	10.43±0.30	51.9 ± 6.3	$-50.0^{+9.2}_{-9.9}$	$-45.6^{+8.0}_{-8.9}$	$-27.5^{+5.3}_{-6.0}$	Hyades	14.75	4	20
2MASS2222-4919	33.76±0.38	100.9 ± 12.3	$-2.3^{+17.7}_{-14.1}$	$-68.0^{+18.8}_{-21.9}$	$-30.6^{+9.6}_{-10.4}$	Pleiades	<10	4	20
2MASS2231-4443	-7.86±0.24	70.7 ± 8.6	$-49.1^{+12.4}_{-14.3}$	$-14.6^{+9.6}_{-11.8}$	$-20.8^{+8.4}_{-9.7}$	IC 2391	<10	4	24
”		46.3 ± 5.6	$-33.6^{+8.2}_{-9.4}$	$-9.3^{+6.3}_{-7.7}$	$-11.3^{+5.6}_{-6.4}$	**Hyades**			
”		52.6 ± 6.4	$-37.6^{+9.3}_{-10.7}$	$-10.7^{+7.2}_{-8.8}$	$-13.8^{+6.3}_{-7.3}$	Castor			
LEHPM4908	-4.15±0.22	49.4 ± 6.0	$-46.4^{+7.6}_{-8.1}$	$-22.8^{+5.3}_{-5.8}$	$-14.7^{+4.4}_{-5.0}$	IC 2391	-	4	21
”		32.3 ± 3.9	$-31.1^{+5.0}_{-5.4}$	$-14.2^{+3.5}_{-3.9}$	$-8.6^{+2.9}_{-3.3}$	**Hyades**			
2MASS2242-2659	2.97±0.21	72.4 ± 8.8	$-24.5^{+8.1}_{-9.5}$	$-16.5^{+7.4}_{-8.9}$	$-19.3^{+4.4}_{-5.1}$	IC 2391	22.14	4	20
”		47.4 ± 5.8	$-15.6^{+5.3}_{-6.2}$	$-10.6^{+4.9}_{-5.8}$	$-13.5^{+3.0}_{-3.4}$	**Hyades**			
”		54.0 ± 6.6	$-17.9^{+6.1}_{-7.1}$	$-12.1^{+5.5}_{-6.6}$	$-15.0^{+3.4}_{-3.8}$	**Castor**			
2MASS2254-3228	0.15±0.55	65.2 ± 7.9	$-6.5^{+6.3}_{-7.8}$	$-29.6^{+9.1}_{-10.7}$	$-6.6^{+3.4}_{-4.0}$	**Pleiades**	18.62	4	22
”		56.5 ± 6.9	$-5.7^{+5.5}_{-6.8}$	$-25.7^{+7.9}_{-9.3}$	$-5.8^{+3.1}_{-3.6}$	**Castor**			
2MASS2311-5256	3.33±0.11	87.3 ± 10.6	$-45.6^{+13.1}_{-15.1}$	$-36.3^{+14.1}_{-16.8}$	$-18.2^{+7.5}_{-9.1}$	Pleiades	<10	2	20
”		101.6 ± 12.4	$-53.3^{+15.3}_{-17.6}$	$-42.2^{+16.4}_{-19.6}$	$-20.7^{+8.8}_{-10.6}$	IC 2391			
”		66.5 ± 8.1	$-34.4^{+10.0}_{-11.6}$	$-27.9^{+10.8}_{-12.8}$	$-14.5^{+5.8}_{-6.9}$	**Hyades**			
SIPS2318-4919	-11.61±0.40	48.9 ± 3.7	$-49.4^{+7.3}_{-7.9}$	$-21.4^{+6.1}_{-6.8}$	$-6.3^{+3.9}_{-4.2}$	**Hyades**	16.50	2	22
SIPS2321-6106	10.31±0.10	64.9 ± 7.9	$-27.4^{+6.5}_{-7.1}$	$-0.8^{+3.8}_{-3.1}$	$-28.6^{+4.4}_{-5.0}$	Pleiades	<10	2	20
”		75.6 ± 9.2	$-32.7^{+7.5}_{-8.3}$	$-0.3^{+4.4}_{-3.6}$	$-32.0^{+5.2}_{-5.8}$	IC3291			
SIPS2322-6357	-8.00±0.26	74.0 ± 9.0	$-39.8^{+8.4}_{-9.5}$	$-20.1^{+7.6}_{-8.9}$	$-3.0^{+4.8}_{-5.7}$	Pleiades	14.77	2	18
”		86.2 ± 10.5	$-45.7^{+9.8}_{-11.1}$	$-23.9^{+8.9}_{-10.4}$	$-4.5^{+5.5}_{-6.6}$	IC 2391			
”		56.4 ± 6.9	$-31.2^{+6.5}_{-7.3}$	$-14.5^{+5.8}_{-6.8}$	$-0.8^{+3.7}_{-4.4}$	**Hyades**			
SIPS2341-3550	-2.76±0.21	56.0 ± 6.8	$-33.7^{+8.4}_{-9.6}$	$-23.3^{+7.4}_{-8.7}$	$-7.3^{+2.8}_{-3.1}$	**IC3291**	14.22	2	23
”		36.7 ± 4.5	$-22.4^{+5.5}_{-6.3}$	$-15.2^{+4.8}_{-5.7}$	$-3.9^{+1.9}_{-2.1}$	Hyades			
”		41.7 ± 5.1	$-25.3^{+6.3}_{-7.2}$	$-17.3^{+5.5}_{-6.5}$	$-4.8^{+2.1}_{-2.4}$	Castor			
SIPS2343-2947	-19.83±0.57	49.3 ± 6.0	$-56.7^{+10.6}_{-11.7}$	$-27.9^{+7.5}_{-8.6}$	$3.6^{+3.4}_{-3.6}$	IC 2391	19.42	2	20
”		32.3 ± 3.9	$-38.8^{+7.0}_{-7.7}$	$-18.8^{+4.9}_{-5.7}$	$9.0^{+2.4}_{-2.6}$	Hyades			

Table 4 – *continued*

Name	$V_r \pm \sigma_{V_r}$ (km s^{-1})	distance (pc)	$U \pm \sigma_U$ (km s^{-1})	$V \pm \sigma_V$ (km s^{-1})	$W \pm \sigma_W$ (km s^{-1})	MG candidature	$V \sin i$ (km s^{-1})	Observing run	S/N
SIPS2347-1821	-6.24±0.32	31.8 ± 3.9	$-32.7^{+6.0}_{-6.6}$	$-10.0^{+3.2}_{-3.7}$	$-1.2^{+1.8}_{-2.0}$	**Hyades**	19.19	2	21
SIPS2350-6915	-6.81±0.48	73.6 ± 9.0	$-53.8^{+12.4}_{-14.1}$	$-17.8^{+9.4}_{-11.3}$	$-11.0^{+7.2}_{-8.6}$	Pleiades	21.20	2	22
”		85.6 ± 10.4	$-62.1^{+14.4}_{-16.3}$	$-21.3^{+10.9}_{-13.1}$	$-13.6^{+8.4}_{-10.0}$	IC 2391			
”		56.1 ± 6.8	$-41.7^{+9.5}_{-10.8}$	$-12.7^{+7.2}_{-8.6}$	$-7.2^{+5.6}_{-6.6}$	**Hyades**			
LEHPM6375	3.63±0.15	37.5 ± 4.6	$-19.7^{+7.5}_{-8.9}$	$-43.9^{+9.8}_{-11.0}$	$-15.1^{+2.8}_{-3.1}$	Sirius	<10	2	25
”		43.3 ± 5.3	$-22.9^{+8.6}_{-10.2}$	$-50.7^{+11.3}_{-12.7}$	$-16.9^{+3.2}_{-3.5}$	Pleiades			
”		50.4 ± 6.2	$-26.7^{+10.0}_{-11.9}$	$-59.1^{+13.1}_{-14.7}$	$-19.1^{+3.6}_{-4.1}$	IC 2391			
”		33.0 ± 4.0	$-17.3^{+6.6}_{-7.8}$	$-38.5^{+8.6}_{-9.7}$	$-13.7^{+2.4}_{-2.7}$	**Hyades**			
”		37.5 ± 4.6	$-19.7^{+7.5}_{-8.9}$	$-43.9^{+9.8}_{-11.0}$	$-15.1^{+2.8}_{-3.1}$	Castor			
LEHPM6542	4.02±0.71	64.7 ± 7.9	$-48.5^{+13.7}_{-15.8}$	$-25.2^{+11.513.7}$	$-15.7^{+4.14.6}$	IC 2391	15.61	2	23
”		42.3 ± 5.2	$-31.6^{+9.0}_{-10.4}$	$-16.2^{+7.6}_{-9.0}$	$-11.7^{+2.9}_{-3.3}$	**Hyades**			
”		48.2 ± 5.9	$-36.0^{+10.2}_{-11.8}$	$-18.5^{+8.6}_{-10.3}$	$-12.7^{+3.2}_{-3.6}$	Castor			

[1] Measused with low S/N
'*' See Sect. 5.3

Eggen O. J., 1984a, AJ 89, 1358
Eggen O. J. 1984b, ApJS, 55, 597
Eggen O. J. 1989, PASP 101, 366
Eggen O. J., 1991, AJ 102, 2028
Eggen O. J., 1992b, AJ 104, 1482
Eggen O. J., 1992c, AJ, 103, 1302
Eggen O. J., 1995, AJ 110, 2862
Eggen O. J., 1998a, AJ 115, 2397
Eggen O. J., 1998b, AJ 116, 782
Famaey B., Pont F., Luri X., Udry S., Mayor M., Jorissen A., 2007, A&A, 461, 957F
Famaey B., Siebert, A., Jorissen A., 200, A&A, 483, 453F
Fischer D. A., Marcy G. W., 1992, ApJ, 396, 178
Francis C., Anderson E., 2009arXiv0901.3503F
Gizis J. E., 2002, ApJ, 575, 484
Gizis J. E., Reid I. N., Knapp G. R., Liebert J., Kirkpatrick J.D., Koerner D.W., Burgasser A. J., 2003, AJ, 125, 3302
Gray D. F. 1992, The Observation and Analysis of Stellar Photospheres, 2nd ed. (Cambridge University Press)
Gorlova N. I., Meyer M. R., Rieke G. H., Liebert J., 2003, ApJ, 593, 1074
Hartmann L., Hewett R., Stahler S., & Mathieu R. D. 1986, ApJ, 309, 275
Hogan E., Jameson R. F., Casewell S. L., Osbourne S. L., Hambly N. C., 2008, MNRAS, 388, 495H
Jameson R. F., Dobbie P. D., Pineld D. J., Hodgkin S. T., 2003, in IAU Symp. 211, ed. E.L. Martín (San Francisco: ASP), p. 1711517
Jenkins J. S., Ramsey L. W., Jones H. R. A., Pavlenko Y., Gallardo J., Barnes J. R., Pinfield D. J., 2009, ApJ, 704, 975
Jenkins J. S., Jones H. R. A., Biller B., O'Toole S. J., Pinfield D. J., Close L., Tinney C.G., Butler R. P., Wittenmyer R., Crter B., Day-Jones A. C., 2010, A&A, 515, 17
Johnson D. R. H., Soderblom D. R., 1987, AJ, 93, 864
Kalnajs A. J., 1991, Dynamics of Disk Galaxies, eds. B. Sundelius, 323
Kaufer A., et al., 1999, The Messenger 95, 8
Kirkpatrick J. D., Henry T. J., McCarthy D. W., 1991, ApJS, 77, 417
Kirkpatrick J. D., Henry T. J., Simons D. A., 1995, AJ, 109, 797
Kirkpatrick J. D et al., 1999, ApJ, 519, 802
Klement R., Fuchs B., Rix H. W., 2008, ApJ, 685, 261K
Knapp G. R., Leggett S. K., Fan X., Marley M. S., Geballe T. R., Golimowski D. A., Finkbeiner D., Gunn J. E. et al., 2004, AJ, 127, 3553
Kornet K., Wolf S., 2006, A&A, 454, 989
Kornet K., Wolf S., Rózyẏczka M., 2006, A&A, 458, 661
Laughlin G., Bodenheimer P., Adams F. C., 2004, ApJ, 612L, 73
Leggett S. K., 1992, ApJS, 82, 351
Lodieu N., Scholz R. D., McCaughrean M. J., Ibata R., Irwin M., Zinnecker H., 2005, A&A 440, 1061
Lyubchik Y., Jones H. R. A., Pavlenko Y. V., Martín E., McLean I. S., Prato L., Barber R. J., Tennyson J., 2007, A&A, 473, 257
López-Santiago J., Micela G., Montes D., 2009, A&A, 499, 129
Martín E. L., Delfosse X., Basri G., Goldman B., Forveille T., Zapatero Osorio M. R., 1999, AJ, 118, 2466
Martín E. L., Barrado Y Navacués D., Baraffe I., Bouy H., Dahm S., 2003, ApJ, 594, 525
Martín E.L., Guenther E., Zapatero Osorio M. R., Bouy H., Wainscoat R., 2006, ApJ, 644L, 75
Mayor M., 1972, A&A, 18, 97
McGovern M. R., Kirkpatrick J. D., McLean I. S., Burgasser A. J., Prato L., Lowrance P. J., 2004, AJ, 600, 1020
Mohanty S., Basri G., 2003, ApJ, 583, 451
Montes D., López-Santiago J., Gálvez M. C., Fernández-Figueroa M. J., De Castro E., Cornide M., 2001, MNRAS, 328, 45
Nidever D. L., Marcy G. W., Butler R. P., Fischer D. A., Vogt S. S., 2002, ApJ, 141, 503
Phan-Bao N., Bessel M. S., 2006, A&A, 446, 51
Pinfield D. J., Dobbie P.D., Jameson R.F., Steele I.A., Jones H. R. A., Ketsiyannis A. C., 2003, MNRAS, 342, 1241
Pinfield D. J., Jones H. R. A., Lucas P. W., Kendall T. R., Folkes S. L., Day-Jones A. C., Chappelle R. J., Steele I. A., 2006, MNRAS, 368, 1281

Table 5. Results: Firts and second columns are name and kinematic classification. Third column classifies the objects as young (Y) if they lie in the upper part of the limiting line in rotational velocity, old (O) if they lie under the line and unknown age (Y-O) if they are in the limit of both areas or the rotational velocity superior limit is not clear enough to classify them in one of the groups. Column four highlights to which MG the candidates are kinematic members. HY for Hyades, SI for Sirius, CA for Castor, PL for Pleiades and IC for IC 2391, and OYD for other young disk members without a membership of one of the five MG in consideration. The '?' marks object where a further spectroscopic study is need to asses or dismiss its membership. (N) markes the two objects that have been dismissed due to the rotational velocity criterion.

Name	Kinematic	$V \sin i$ Classification	Possible MG membership
SIPS0004-5721	YD	Y	**HY, IC**
SIPS0007-2458	YD	Y	**IC**
2MASS0020-2346	YD	Y	**OYD**
DENIS0021-4244	YD	O	(N)
SIPS0027-5401	YD	Y	**HY**
SIPS0039-2256	YD	Y-O	**OYD?**
DENIS0041-5621	YD	Y	**OYD**
SIPS0054-4142	YD	Y-O	**OYD?**
SIPS0109-0343	YD	O	-
LEHPM1289	OD	Y	-
SIPS0115-2715	OD	Y-O	-
2MASS0123-3610*	YD	Y	**HY**
SIPS0126-1946	OD	Y	-
LEHPM1563	YD	Y	**OYD**
SIPS0153-5122	YD	Y	**HY, IC**
2MASS0204-3945	YD	O	(N)
SIPS0212-6049	OD	Y-O	-
SIPS0214-3237	YD	Y	**HY**
SIPS0235-0711	YD	Y	**HY**
2MASS0334-2130	YD	Y-O	**IC?**
2MASS0429-3123	YD	O	-
SIPS0440-0530	YD	Y	**HY**
2MASS0445-5321	OD	-	-
2MASS0502-3227	OD	Y-O	-
2MASS0528-5919	OD	Y-O	-
2MASS0600-3314	YD	-	**HY?**
SIPS1039-4110	YD	-	**OYD?**
SIPS1124-2019	YD	-	-
DENIS1250-2121	OD	-	-
SIPS1329-4147	OD	-	-
SIPS1341-3052	OD	-	-
2MASS1507-2000	OD	-	-
SIPS1632-0631	OD	O	-
SIPS1758-6811	OD	Y	-
SIPS1949-7136	OD	-	-
SIPS2000-7523	YD	-	**CA?**
2MASS2001-5949	OD	Y	-
SIPS2014-2016	YD	Y	**HY**
2MASS2031-5041	YD	Y	**HY**
SIPS2039-1126	YD	Y	**PL**
SIPS2045-6332	YD	Y-O	**CA, PL?**
SIPS2049-1716	YD	-	**HY?**
SIPS2049-1944	YD	Y	**OYD**
SIPS2100-6255	YD	-	**HY?**
2MASS2106-4044	OD	Y	-
SIPS2114-4339	YD	Y	**CA**
SIPS2119-0740	OD	Y	-
HB2124-4228	YD	Y	**PL**
SIPS2128-3254	YD	Y	**OYD**
DENIS2200-3038	YD	O	HY?
SIPS2200-2756	YD	Y-O	**HY?**
2MASS2207-6917	YD	Y	**HY**
LEHPM4480	OD	Y	-
2MASS2222-4919	OD	O	-
2MASS2231-4443	YD	Y	**HY**
LEHPM4908	YD	-	**HY?**
2MASS2242-2659	YD	Y	**CA, HY**
2MASS2254-3228	YD	Y	**CA, PL**
2MASS2311-5256	YD	Y	**HY**
SIPS2318-4919	YD	Y	**HY**
SIPS2321-6106	YD	Y	**OYD**
SIPS2322-6357	YD	Y	**HY**
SIPS2341-3550	YD	Y	**IC**
SIPS2343-2947	YD	Y	**OYD**
SIPS2347-1821	YD	Y	**HY**
SIPS2350-6915	YD	Y	**HY**
LEHPM6375	YD	Y-O	**HY?**
LEHPM6542	YD	Y	**HY**

'*' See Sect. 5.3

Reid I. N., Lewitus E., Allen P. R., Cruz K. L., Burgasser A. J., 2006, AJ, 132, 891
Reiner A., Basri G. 2008, AJ, 684, 1390
Reiners A., Basri G. 2009, ApJ, 705, 1416R
Ribas I., 2003, A&A, 398, 239
Ribas I., 2003b, A&A, 400, 297
Rhode K. L., Herbst W., Mathieu R. D. 2001, AJ, 122, 3258
Seifahrt A., Reiners A., Almaghrbi K. A. M., Basri G. 2010, A&A, arXiv:1001.1780v1
Siegler N., Close L., Cruz K. L., Martín E. L., Reid I. N., 2005, 621, 1023
Skuljan J., Hearnshaw J. B., Cottrell P. L., 1999, MNRAS, 308, 731
Soderblom D. R., Mayor M., 1993a, AJ, 105, 226
Soderblom D. R., Mayor M., 1993b, ApJ, 402L, 5
Spezzi L., Pagano I., Marino G., Leto G., Young E., Siegler N., Balog Z., Messina S., Distefano E., Merín B., Barrado y Navascués D., 2009, A&A, 499, 541S
Tinney, 1996, MNRAS, 281, 644
Tonry J., Davis M. 1979, AJ, 84 1511
West A. A., Hawley S. L., Bochanski J. J., Covey K. R., Reid I. N., Dhital S., Hilton E. J., Masuda M., 2008, AJ, 135, 785
Zhao J., Zhao G., Chen Y., 2009, ApJ, 692L, 113Z
Zapatero-Osorio M. R., Lane B. F., Pavlenko Ya., Martín E. L., Britton M., Kulkarni S. R., 2004, ApJ, 615, 958
Zapatero-Osorio M. R., Martín E. L., Bouy H., Tata R., Deshpande R., Wainscoat R. J., 2006, AJ, 647, 1405
Zhang Z. H., Pinfield D. J., Day-Jones A. C., Burningham B., Jones H. R. A., Yu s., Jenkins J. S., Han Z., Gálvez-Ortiz M. C., Gallardo J., García Pérez A. E., Weights D. J., Tinney C. G., Pokorny R. S., 2010, arXiv1001.3609Z

This paper has been typeset from a TEX/ LATEX file prepared by the author.